Water Resources Research

RESEARCH ARTICLE
10.1029/2018WR023485

**Key Points:**
- We evaluated the MOD16 algorithm based on data from 175 flux towers
- We acquired optimized parameters for the MOD16 algorithm via the DE-MC scheme
- We evaluated and compared the results at multiple temporal and spatial scales

**Supporting Information:**
- Supporting Information S1

**Correspondence to:**
J. Ma,
jzma@lzu.edu.cn

**Citation:**
Zhang, K., Zhu, G., Ma, J., Yang, Y., Shang, S., & Gu, C. (2019). Parameter analysis and estimates for the MODIS evapotranspiration algorithm and multiscale verification. *Water Resources Research*, *55*, 2211–2231. https://doi.org/10.1029/2018WR023485

Received 12 JUN 2018
Accepted 18 FEB 2019
Accepted article online 25 FEB 2019
Published online 20 MAR 2019



# Parameter Analysis and Estimates for the MODIS Evapotranspiration Algorithm and Multiscale Verification

**Kun Zhang[1,2], Gaofeng Zhu[1], Jinzhu Ma[1], Yuting Yang[3], Shasha Shang[1], and Chunjie Gu[1]**

[1]Key Laboratory of Western China's Environmental Systems (Ministry of Education), College of Earth and Environmental Sciences, Lanzhou University, Lanzhou, China, [2]Institute of Tibetan Plateau Research, Chinese Academy of Sciences, Beijing, China, [3]State Key Laboratory of Hydroscience and Engineering, Department of Hydraulic Engineering, Tsinghua University, Beijing, China

**Abstract** Accurate estimation of terrestrial evapotranspiration (*E*) is critical to understand the world's energy and water cycles. MOD16 is the core algorithm of the widely used global *E* data set (the Moderate Resolution Imaging Spectroradiometer [MODIS] *E* product). However, it exhibits considerable uncertainties in some regions. Based on the data from 175 flux towers, we identified the key parameters of the MOD16 algorithm using the Sobol' sensitivity analysis method across biomes. The output of the MOD16 algorithm was sensitive to eight parameters. Among them, β, which is treated as a constant (0.2 kPa) across biomes in the original MOD16 algorithm, was identified as the parameter to which the algorithm was most sensitive. We used the differential-evolution Markov chain method to obtain the proper posterior distributions for each key parameter across a range of biomes. The values of the key parameters for the different biomes were accurately estimated by differential-evolution Markov chain in comparison with data from the flux towers. We then evaluated the performances of the original MOD16 and the optimized MOD16 and compared them at multiple spatial scales (i.e., site, catchment, and global). We obtained relatively consistent and more reliable *E* simulations using the optimized MOD16 at all three scales. In the future, more attention should be paid to uncertainties in the algorithm's structure and its parameterizations of soil moisture constraint, canopy resistance, and energy partitioning.

## 1. Introduction

Terrestrial evapotranspiration (*E*) is a key component of the global hydrological cycle and functions as a nexus that links the exchanges of water, carbon, and energy between the biosphere and the atmosphere (Jung et al., 2011; Wang & Dickinson, 2012). Thus, accurate quantification of *E* and its spatial and temporal patterns are crucial for understanding regional water and energy balances and improving practical applications of the associated processes in irrigation and water resource management (Morillas et al., 2013; Oki & Kanae, 2006; Yang et al., 2012; Zhang et al., 2016). Over the past few decades, numerous models of *E* based on satellite remote sensing have been developed to allow mapping of *E* from regional to global scales, primarily due to the ability of satellite sensors to efficiently capture land surface information over very large scales, including at a global scale. The majority of these models can be broadly categorized into three groups: surface energy-balance models (Bastiaanssen et al., 1998; Norman et al., 1995; Su, 2002), vegetation index (VI)-land surface temperature (LST) triangle/trapezoidal models (Jiang & Islam, 1999; Long & Singh, 2012; Yang & Shang, 2013), and Penman-Monteith (PM) or Priestley-Taylor (PT) models (Cleugh et al., 2007; Fisher et al., 2008; Leuning et al., 2008; Miralles et al., 2011; Mu et al., 2007, 2011; Zhang, Kimball, et al., 2010; Zhang, Leuning, et al., 2010). The first two types are commonly based on remotely sensed LST. They first calculate the sensible heat flux based on the difference between LST and air temperature, then regard the latent heat flux (or its water equivalent, *E*) as a residual in the surface energy-balance equation. In contrast, the PM- or PT-based models do not require LST as a model input. Instead, they estimate *E* (or its two components, evaporation and transpiration) directly from PM- or PT-type equations, in which the required surface conductance is expressed as a function of a remotely sensed VI and concurrent meteorological conditions.

Among those models, the PM-based models have been widely used in hydrological, ecological, and climatological studies (e.g., Chen et al., 2014; Ershadi et al., 2014, 2015; Hu et al., 2015; Long et al., 2014; McCabe et al., 2016; Mueller et al., 2013; Ramoelo et al., 2014; Vinukollu et al., 2011; Yang et al., 2014; Zhang

et al., 2008, 2015). This is because they offer the advantage of estimating *E* directly at daily or longer time scales. This effectively avoids the uncertainty that arises when upscaling *E* values from an instantaneous scale (a snapshot at the time of the satellite overpass) to longer scales, which is required in both energy-balance residual models and VI-LST space models (Ryu et al., 2012). MOD16 is the underlying algorithm of the *E* product produced by the Moderate Resolution Imaging Spectroradiometer (MODIS). The algorithm calculates plant transpiration, soil, and canopy intercepted evaporation separately using a set of PM-type equations, in which the conductance terms (i.e., aerodynamic and canopy surface conductance) and soil surface moisture constraints are estimated from a set of semiempirical equations that have been developed for different land cover types (Mu et al., 2011).

On the one hand, these semiempirical equations are relatively easy to implement and thus allow operational application of MOD16 at a global scale. On the other hand, these semiempirical functions require calibration against actual *E* measurements, and their performances depends on the amount of *E* data and the representativeness of the observation sites that provided these data for each land cover type. The latest version of the MOD16 algorithm (Mu et al., 2011), which represents an improvement over the original version of Mu et al. (2007) based on methods originally developed by Cleugh et al. (2007), was calibrated against *E* observations from 46 flux sites in the AmeriFlux network (http://ameriflux.lbl.gov/). However, subsequent studies showed that MOD16 performs suboptimally, and in a few cases unacceptably, in many regions of the world (Ershadi et al., 2015; Kim et al., 2012; Ramoelo et al., 2014; Trambauer et al., 2014; Velpuri et al., 2013; Yang et al., 2015; Yao et al., 2014). This is partly due to the limited and geographically biased observations that Mu et al. (2011) used to calibrate MOD16 (they used only 46 sites, and all of the sites were located in North America). This suggests that the original parameters of MOD16 may be unsatisfactory, especially for regions outside of North America. In this light, it is imperative to recalibrate the algorithm and optimize its parameters using a more comprehensive collection of site-specific *E* data that cover the range of global bioclimatic conditions (McCabe et al., 2016). In addition, the intrinsic parameter had been proved with significant influence on the simulation process (Michel et al., 2005). The parameter $\beta$ in MOD16 is treated as an intrinsic parameter and holds constant across global bioclimate conditions. However, previous studies have illustrated that its values have significant influences on the soil evaporation estimations (Yang et al., 2015; Zhang et al., 2017). Thus, it is urgently needed to investigate its influence on the simulation process and identify its proper values across global bioclimates for improving the performance of MOD16.

Sensitivity analysis is a powerful tool for understanding the importance of model parameters in terms of how variations in their values affect model outputs and for optimizing the model parameters (Nossent et al., 2011; Zhang et al., 2017; Zhu et al., 2016). In conventional hydrological and ecological model analysis, the one-fact-at-a-time (OAT) method, in which one parameter is changed at a time while fixing others, has been widely used to assess the sensitivity of models to the values of their parameters (Bouda et al., 2014; van Griensven et al., 2006). However, despite its low computational cost, the OAT method has been shown to produce highly biased results when it is applied to high-dimension and nonlinear systems (Yang, 2011), which is a common case in environmental modeling. To solve that problem, global sensitivity analysis (GSA) has been used, as it is designed for exploring the sensitivity of models to their parameters over the entire parameter space, and is therefore more suitable for environmental models that consist of a set of nonlinear processes, such as those in the MOD16 algorithm (Pappenberger et al., 2008; Vanrolleghem et al., 2015; Zhang et al., 2013). Recently, various GSA methods have been developed for use with hydrological and environmental models and have shown improved ability to quantify model sensitivity to parameters compared with the OAT method (Confalonieri et al., 2010; Foscarini et al., 2010; Nossent et al., 2011; Tang et al., 2007).

For parameter optimization, Bayesian-based methods have gained considerable attention from the environmental modeling community because they provide a powerful tool from which inferences can be drawn (Clark & Gelfand, 2006; Huisman et al., 2010; Keating et al., 2010; Zhu et al., 2014). However, conventional Bayesian-based methods, such as Markov-chain Monte Carlo (MCMC) analysis, often suffer from problems related to selection of an appropriate scale and orientation for the jumping distribution, which may prevent the algorithm from efficiently converging (Haario et al., 2006; Vrugt et al., 2009). Alternatively, the differential-evolution Markov chain (DE-MC) method (Ter Braak, 2006; Ter Braak & Vrugt, 2008) combines a genetic algorithm (Storn & Price, 1997) with the MCMC method. Multiple Markov chains are constructed in the DE-MC method to estimate the posterior distribution of the parameters, which has the advantage that

it can effectively avoid the problem of achieving local convergence that occurs with single chains and can greatly improve the computational efficiency. Hence, the DE-MC method is a more suitable tool for use with the high-dimensional models, from which inferences are drawn in environmental and hydrological sciences (Smith & Marshall, 2008; Ter Braak & Vrugt, 2008). Nevertheless, no studies have been conducted using the DE-MC method to optimize the parameters of the MOD16 algorithm.

In this study, we investigated the sensitivity of MOD16 to the values of its parameters so that we could identify its key parameters and optimize their values using $E$ observations from eddy covariance towers around the world. Specifically, our objectives were to (i) identify and analyze the key parameters in MOD16 that were specific to different land cover types, (ii) optimize the values of the key model parameters and use them to generate a global terrestrial daily $E$ data set, and (iii) comprehensively evaluate the new MOD16 $E$ estimates across multiple spatial scales (i.e., site, catchment, and global scales) by comparing them with the results of the original MOD16.

## 2. Methods

### 2.1. Review of the MOD16 Algorithm

The MOD16 algorithm calculates the actual evaporation from the soil ($E_s$) and wet canopy (i.e., canopy intercepted evaporation; $E_{wet}$) and the plant transpiration ($E_t$) individually based on PM-type equations. The total evapotranspiration is the sum of these three components:

$$E = E_{wet} + E_s + E_t \tag{1}$$

where

$$E_{wet} = \frac{(\Delta \cdot R_{nc} + \rho \cdot C_P \cdot f_c \cdot VPD/r_{hrc}) \cdot f_{wet}/\lambda}{\Delta + (P_a \cdot C_P \cdot r_{vc})/(\lambda \cdot \varepsilon \cdot r_{hrc})} \tag{2}$$

$$E_s = \frac{(\Delta \cdot R_{ns} + \rho \cdot C_P \cdot (1-f_c) \cdot VPD/r_{as})/\lambda}{\Delta + \gamma \cdot r_{tot}/r_{as}} \cdot [f_{wet} + (1-f_{wet}) \cdot f_{sm}] \tag{3}$$

$$E_t = \frac{(\Delta \cdot R_{nc} + \rho \cdot C_P \cdot f_c \cdot VPD/r_a) \cdot (1-f_{wet})/\lambda}{\Delta + \gamma \cdot (1 + r_s)/r_a} \tag{4}$$

In equations (2) to (4), $\Delta$ is the slope of the saturated vapor-pressure curve (kPa/°C), $\rho$ is the air density (kg/m$^3$), $C_p$ is the specific heat capacity of air (MJ · kg$^{-1}$ · °C$^{-1}$), $\lambda$ is the latent heat of evaporation (MJ/kg), $\varepsilon$ is the ratio of the molecular weight of water to dry air (i.e., 0.622), $\gamma$ is the psychrometric constant (kPa/°C), $P_a$ is the atmospheric pressure (kPa), and $VPD$ is the atmospheric vapor-pressure deficit (kPa). $R_{nc}$ and $R_{ns}$ (W/m$^2$) are the net radiation allocated to the canopy and soil surfaces, respectively, which are calculated based on the whole-surface net radiation ($R_n$) weighted by the relative areas of each component. $f_c$ is the fractional vegetation cover (dimensionless), and $f_{wet}$ is the relative surface wetness (equal to the fourth power of relative humidity, $RH^4$).

In estimating $E_{wet}$ (i.e., equation (2)), $r_{vc}$ and $r_{hrc}$ represent the surface resistance (s/m) and aerodynamic resistance (s/m) to evaporated water on the wet canopy surface, respectively, and are quantified by the following equations:

$$r_{vc} = \frac{1}{g_{l\_e\_wv} \cdot LAI \cdot f_{wet}} \tag{5}$$

$$r_{hrc} = \frac{r_{hc} \cdot r_{rc}}{r_{hc} + r_{rc}} \tag{6}$$

$$r_{hc} = \frac{1}{g_{l\_sh} \cdot LAI \cdot f_{wet}} \tag{7}$$

$$r_{rc} = \frac{\rho \cdot C_P}{4 \cdot \sigma \cdot T_i^3} \tag{8}$$

where $T_i$ represents the daytime or nighttime average temperature (°C), LAI is the leaf area index (leaf area per unit ground area covered by the leaves), $\sigma$ is the Stefan-Boltzmann constant (i.e., $5.6704 \times 10^{-8}$, $W \cdot m^{-2} \cdot K^{-4}$), $r_{hc}$ is the wet canopy resistance to sensible heat, and $r_{rc}$ is the resistance to radiative heat transfer through air (s/m). There are two basic parameters (Table 1; dotted boxes in Figure 1) in the wet canopy surface section: $g_{l\_e\_wv}$ and $g_{l\_sh}$, that represent the leaf conductance for evaporated water vapor and the sensible heat per unit LAI, respectively (m/s).

In estimating $E_s$ (i.e., equation (3)), $r_{tot}$ is the total aerodynamic resistance (s/m), which represents the sum of the surface resistance and the aerodynamic resistance for vapor transport, and $r_{as}$ is the aerodynamic resistance at the soil surface (s/m):

$$r_{tot} = r_{totc} \cdot r_{corr} \tag{9}$$

$$r_{as} = \frac{r_{rs} \cdot r_{hs}}{r_{rs} + r_{hs}} \tag{10}$$

$$r_{totc} = \begin{cases} rbl_{min} & VPD \le VPD_{open} \\ rbl_{max} - \dfrac{(rbl_{max} - rbl_{min}) \cdot (VPD_{close} - VPD)}{VPD_{close} - VPD_{open}} & VPD_{open} \le VPD \le VPD_{close} \\ rbl_{max} & VPD \ge VPD_{open} \end{cases} \tag{11}$$

where $r_{totc}$ is an initial value for $r_{tot}$, which can be calculated by a segmented function of $VPD$ with a maximum limit ($rbl_{max}$) and a minimum limit ($rbl_{min}$), and $r_{corr}$ is a correction coefficient based on air temperature and pressure. The aerodynamic resistance at the soil surface ($r_{as}$) is derived from $r_{rs}$ (the resistance to radiative heat transfer, which is the same as $r_{rc}$ in the equation (8)) and $r_{hs}$ (the resistance to convective heat transfer, which is equal to $r_{tot}$).

The term $f_{sm}$ is the constraint to soil evaporation, which is an index of soil water deficit based on the complementary hypothesis (Bouchet, 1963; Fisher et al., 2008) as a function of relative humidity ($RH$, %) and $VPD$ (kPa):

$$f_{sm} = RH^{VPD/\beta} \tag{12}$$

where $\beta$ is the sensitivity of $f_{sm}$ to $VPD$ and was set as a constant of 0.2 (kPa) by Mu et al. (2011). However, previous studies have noted that the value of $\beta$ should change to account for differences among land cover types and climate conditions (Yang et al., 2015). For example, Zhu et al. (2016) have shown that the model performs better using a low value ($\beta = 0.1$) for water-limited ecosystems. Thus, in this study, we regarded $\beta$ as a variable rather than as a constant (Table 1; dotted box in Figure 1) and included it in the optimization calculations.

In estimating $E_t$ (equation (4)), $r_a$ is the aerodynamic resistance between the mean canopy height (s/m) and the air above the canopy and $r_s$ is the canopy surface resistance (s/m), which are estimated by

$$r_a = \frac{r_h \cdot r_r}{r_h + r_r} \tag{13}$$

$$r_s = \frac{1}{C_c} \tag{14}$$

$$r_h = \frac{1}{g_{l\_bl}} \tag{15}$$

$$C_c = \frac{g_{l\_sh} \cdot (G_s + G_{cu})}{G_s + g_{l\_sh} + G_{cu}} \cdot LAI \cdot (1 - f_{wet}) \tag{16}$$

$$G_s = C_l \cdot m(T_{min}) \cdot m(VPD) \cdot r_{corr} \tag{17}$$

$$G_{cu} = g_{cu} \cdot r_{corr} \tag{18}$$

**Table 1**
*The Descriptions and Prior Ranges of the Parameters in the MOD16 Algorithm That Were Used in the Sensitivity Analysis and Optimization Calculations*

| Parameter | Description | Intermediate variable | Prior range | Unit |
|---|---|---|---|---|
| $T_{min\_open}$ | Minimum temperature that has no inhibition of transpiration | $r_s \rightarrow E_T$ | [4, 18] | °C |
| $T_{min\_close}$ | Minimum temperature that has nearly complete inhibition of transpiration | $r_s \rightarrow E_T$ | [−12, −3] | °C |
| $VPD_{close}$ | *VPD* that has nearly complete inhibition of transpiration | $r_s \rightarrow E_T$; $r_{as} \rightarrow E_s$ | [1450, 6500] | kPa |
| $VPD_{open}$ | *VPD* that has no inhibition of transpiration | $r_s \rightarrow E_T$; $r_{as} \rightarrow E_s$ | [325, 1500] | kPa |
| $g_{l\_sh}$ | Leaf conductance of sensible heat per unit LAI | $r_{hrc} \rightarrow E_{wet}$; $r_s$ & $r_a \rightarrow E_T$ | [0.005, 0.12] | m/s |
| $g_{l\_e\_wv}$ | Leaf conductance of evaporated water vapor per unit LAI | $r_{vc} \rightarrow E_{wet}$ | [0.005, 0.12] | m/s |
| $C_l$ | Mean potential stomatal conductance per unit leaf area | $r_s \rightarrow E_T$ | [0.0013, 0.0105] | m/s |
| $rbl_{min}$ | Minimum value for total aerodynamic resistance of soil | $r_{as} \rightarrow E_s$ | [10, 105] | s/m |
| $rbl_{max}$ | Maximum value for total aerodynamic resistance of soil | $r_{as} \rightarrow E_s$ | [20, 150] | s/m |
| β | A sensitivity index for the soil constraint on *VPD* | $f_{sm} \rightarrow E_s$ | [0, 1] | kPa |

*Note.* $r_s$ and $r_a$ are the surface resistance and aerodynamic resistance of the dry canopy, $r_{vc}$ and $r_{hrc}$ are the surface resistance and aerodynamic resistance of the wet canopy, and $r_{as}$ is the aerodynamic resistance of soil. LAI, leaf area index; VPD, vapor-pressure deficit.

$$r_{corr} = \frac{P}{101.3} \cdot \left(\frac{T_i + 273.15}{293.15}\right)^{-1.75} \tag{19}$$

where $r_r$ is the radiative heat transfer resistance, which is the same as $r_{rc}$ (s/m), $r_h$ is the convective heat transfer resistance (s/m), and $g_{l\_bl}$ is the leaf boundary layer conductance (m/s), which is equal to $g_{l\_sh}$ in the previous equations. $C_c$ is the surface conductance ($m/s^1$), $G_s$ is the stomatal conductance (m/s), $g_{cu}$ is the cuticular conductance per unit LAI (m/s), and $C_l$ is the mean potential stomatal conductance per unit LAI (m/s). In this section, $g_{l\_bl}$, $g_{l\_sh}$, $C_l$, and the four climate thresholds (i.e., $T_{min\_close}$, $T_{min\_open}$, $VPD_{close}$, and $VPD_{open}$) are used as the basic parameters (Figure 1 and Table 1). Further details of the MOD16 algorithm and its parameters are available in Mu et al. (2007, 2011).

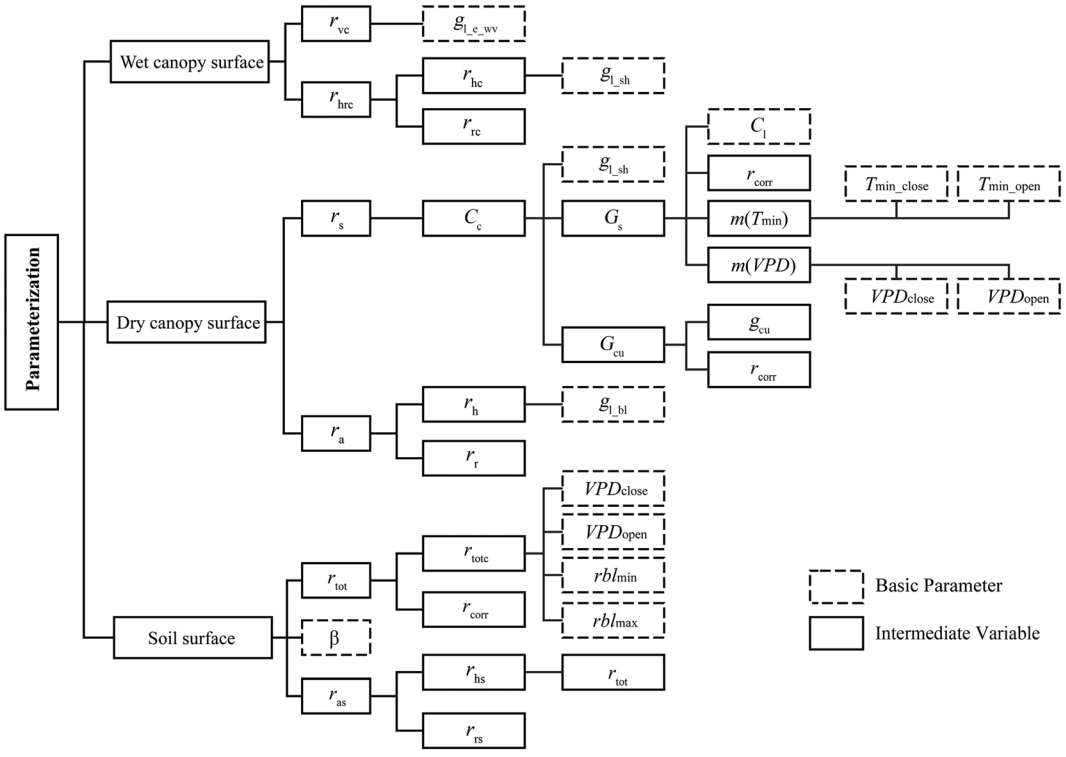


**Figure 1.** Parameterization scheme of the MOD16 algorithm. Basic parameters are the parameters for which we conducted the sensitivity analysis.

### 2.2. Global Sensitivity Analysis

In this study, we adopted the method of Sobol (Sobol', 1990, 2001) to calculate the sensitivity index (SI) of the basic parameters in MOD16. This method is a GSA approach based on variance decomposition and is applicable to nonlinear and nonmonotonic models or algorithms. A parameterized model (algorithm) can be represented by the following functional form.

$$y = f(X, \theta) \tag{20}$$

where $y$ is the output of the model (or the objective function), $\theta$ is the model parameter, and $X$ is the forcing data of the model. In the Sobol' method, the total variance of function $f$ can be decomposed into a summation of terms with increasing dimensionality:

$$D(y) = \sum_{i=1}^{k} D_i + \sum_{i=1}^{k-1} \sum_{j=i+1}^{k} \left(D_{ij} + \cdots + D_{1,\cdots,k}\right) \tag{21}$$

where $D(y)$ is the partial variance for the first-order sensitivity of $\theta_i$ for the model output $y$, $D_{ij}$ is the partial variance for the second-order sensitivity for the $i$th and $j$th parameter interactions, and $k$ is the total number of parameters. The final sensitivity effect is divided into a first-order sensitivity, a second-order sensitivity, and a total-order sensitivity, which are characterized by the ratio of the partial variances to the total variance. Further details about the method can be found in the supporting information, and also available in Nossent et al. (2011).

### 2.3. Parameter Optimization With a Differential-Evolution Markov Chain

When the observed data are fixed in a Bayesian framework, the posterior distribution of a parameter is generally proportional to the corresponding prior distribution of the parameter, multiplied by a likelihood function:

$$p(\theta|O) \propto p(O|\theta)p(\theta) \tag{22}$$

where $O$ is the observed data, $\theta$ is the parameter, $p(\theta|O)$ is the posterior distribution of the parameter, $p(\theta)$ is the prior distribution of the parameter (uniform distribution in this study), and $p(O|\theta)$ is the likelihood function that reflects the effect of the observed data on the parameter identification and can be expressed as follows (Zhu et al., 2014):

$$p(O(t)|\theta) = \prod_{t=1}^{T} \frac{1}{\sqrt{2\pi\sigma^2}} \exp\left(-\frac{(O(t)-S(t))^2}{2\sigma^2}\right) \tag{23}$$

where $T$ is the total number of observed data, $O(t)$ is the observed data at time $t$, $S(t)$ is the simulated data at time $t$, $\pi$ is a mathematical constant approximately equal to 3.1416, and $\sigma$ is the standard deviation of the model error during the observed period and is regarded as fixed (Braswell et al., 2005).

In this study, we estimated the posterior distribution (i.e., equation (22)) using the DE-MC scheme, which is an adaptive MCMC algorithm that has been proposed for global optimization in real parameter spaces by combining multiple chains that are running in parallel (Ter Braak & Vrugt, 2008). In DE-MC, the proposals are generated based on two chains that are randomly selected from multiple chains, and the difference between the two chains is multiplied by a scaling factor $\gamma$ and then added to the current chain:

$$\theta_p = \theta_i + \gamma(\theta_{r1} - \theta_{r2}) + e \tag{24}$$

where $\theta_p$ is the proposed parameter; $\theta_{r1}$ and $\theta_{r2}$ are the two randomly selected chains running in parallel; $\gamma$ is the scaling factor, which can be set as $2.38/\sqrt{2d}$ where $d$ is the dimension of the parameter; and $e$ is drawn from a symmetrical distribution and represents a probabilistic acceptance rule in the DE-MC. For example, $e \sim N(0, b)^2$ for small $b$, where $N$ represents a normal distribution. In the present analysis, we ran 20 chains in parallel with 8000 iterations, including 500 iterations as a burn-in period.

More specifically, we first used the DE-MC to obtain a set of optimized parameters (the median values of the posterior distributions) for each site and calculated the site-level root-mean-square error (S-RMSE) based on

the difference between the observed and simulated values (which were obtained by optimized parameters). By the end of this step, the posterior distributions of the parameters for each biome will be substantially lower than their prior distributions (Zhang et al., 2017; Zhu et al., 2014). Next, we used the DE-MC again to obtain a set of parameters that was suitable for both the site and biome levels. That is, we randomly selected a set of parameters from the parameter space obtained in the first step. We then calculated the root-mean-square error (RMSE) values for all sites that belonged to a given biome and compared the results with the S-RMSE values. This cycle of comparisons was repeated until the values of the RMSE became closest to the S-RMSE values for the biome (i.e., until the analysis achieved convergence). This procedure ensured that the optimized parameters had an optimal balance for each site that belonged to a specific biome.

### 2.4. Evaluation and Objective Function

The parameter sensitivity analysis and optimization need a goodness-of-fit metric to address the uncertainty and errors in the simulation. We chose the RMSE as the objective function to be minimized. Moreover, we quantified mismatches between the model and the data at the site and biome levels using Pearson's correlation coefficient ($r$), the slope of the model, its $y$ intercept, its bias, its relative error (RE), and the Nash-Sutcliffe efficiency coefficient (NSE; Legates & McCabe, 1999; Nash & Sutcliffe, 1970). These statistics were calculated as follows:

$$\text{Bias} = \frac{1}{T}\sum_{t=1}^{T}[O(t)-S(t)] \tag{25}$$

$$\text{RMSE} = \sqrt{\frac{1}{T}\sum_{t=1}^{T}[O(t)-S(t)]^2} \tag{26}$$

$$\text{RE} = \frac{\text{RMSE}}{\overline{O}} \tag{27}$$

$$\text{NSE} = 1-\frac{\sum_{t=1}^{T}[O(t)-S(t)]^2}{\sum_{t=1}^{T}\left[O(t)-\overline{O}\right]^2} \tag{28}$$

where $\overline{O}$ is the mean of the observed data and NSE is used to quantitatively describe the accuracy of the model outputs other than the observed data with a range from $-\infty$ to 1. Generally, the closer the NSE is to 1, the more accurate the simulation is.

Additionally, we used Taylor diagrams (Taylor, 2001) to characterize the model's performance. Each single point in the diagram represents the correlation coefficient ($r$), the normalized standard deviation (the ratio of the standard deviation of the simulated values to the standard deviation of the observations). It can be scored as

$$S = \frac{2(1+r)}{[(\sigma_s/\sigma_o)+1/(\sigma_s/\sigma_o)]^2} \tag{29}$$

where $S$ is the model skill metrics bounded by zero and unity (i.e., unity indicates perfect agreement with the observations) and $\sigma_s$ and $\sigma_o$ are the standard deviations of the simulated and observed data, respectively.

## 3. Data

### 3.1. Input Data

#### 3.1.1. Remote-Sensing Data

To characterize the state of the land surface vegetation and its radiation absorption, and to generate the $E$ data set at a global scale, we used three sets of MODIS remote-sensing products from 2001 to 2006:

(i) The LAI and the fraction of photosynthetically active radiation absorbed by green vegetation ($f_{PAR}$) from the MCD15A2 product at a 1-km spatial resolution and an 8-day temporal interval.

(ii) The surface albedo from the MCD43C1 product (band 10 of the white-sky albedo) at a 0.05° spatial resolution and a daily temporal interval.
(iii) The land cover type from the MCD12C1 product (band 1 of the IGBP classification) at a 0.05° spatial resolution and an annual temporal interval.

These products were acquired from the Land Processes Distributed Active Archive Center (https://lpdaac.usgs.gov/dataset_discovery/modis) and were reprojected onto the WGS84 grid and spatially resampled to a 0.05° spatial resolution before using them as the forcing values. In addition, we performed temporal interpolation of the remote-sensing product based on the method proposed by Zhao et al. (2005) to obtain data for the pixels with low data quality or missing data (i.e., based on the quality control band of these products), which was caused primarily by cloud contamination.

#### 3.1.2. Meteorological Data

We chose the Modern-Era Retrospective analysis for Research and Applications Version 2 (MERRA-2, Gelaro et al., 2017) from National Aeronautics and Space Administration (NASA)'s Global Modeling and Assimilation Office (https://disc.sci.gsfc.nasa.gov) to provide global meteorological data at a spatial resolution of 0.5° × 0.625° and a daily temporal interval. This data set included near-surface air pressure and temperature, specific humidity, and downward shortwave radiation.

To match the MODIS spatial resolution, we performed spatial interpolation of the surface meteorological data based on the nonlinear spatial interpolation method proposed by Zhao et al. (2005). In brief, this method used a cosine function raised to the fourth power to separately obtain the nonlinear distance based on the *great circle distance* between the four MERRA-2 pixels surrounding a given MODIS pixel and the MODIS pixel. We then acquired the interpolated result for a given pixel from the weighted value of the four coarse pixels, which were based on the nonlinear distance. This spatial interpolation is logical and accurate because it eliminates the abrupt boundary changes between the coarse MERRA-2 pixels (Mu et al., 2011; Zhao et al., 2005).

### 3.2. Global *E* Data for Model Calibration and Evaluation

#### 3.2.1. Site-Scale *E* Values

We used a total of 175 flux sites from FLUXNET (Baldocchi et al., 2001; Jung et al., 2009) to identify the parameters to which the MOD16 algorithm was most sensitive so that we could optimize these parameters. These sites represent a wide range of land cover types (from the MODIS IGBP classification, https://modis.gsfc.nasa.gov/data/dataprod/mod12) and were distributed throughout the world (Figure 2). They included the following biomes: evergreen needleleaf forest (ENF, 46 sites), evergreen broadleaf forest (EBF, 14 sites), deciduous needleleaf forest (DNF, 1 sites), deciduous broadleaf forest (DBF, 25 sites), mixed forest (MF, 6 sites), closed shrubland (CSH, 3 sites), open shrubland (OSH, 13 sites), woody savanna (WSA, 6 sites), savanna (SAV, 7 sites), grassland (GRA, 36 sites), and cropland (CRO, 18 sites).

The flux data used in this study are all available from the FLUXNET database (at https://fluxnet.fluxdata.org). We adjusted some of the flux data to ensure the quality of the data used in this study. The energy closure for site is a key indicator of the quality of the flux data (Zhu et al., 2016). The flux data for a 30-min period (for some sites, 60 min) were treated as missing if the energy imbalance (net radiation minus the sum of the latent, sensible, and ground heat flux) exceeded 300 $W/m^2$. In addition, if data gaps were less than 6 hr in a day, the missing data were linearly interpolated. After performing these adjustments, the energy-balance closure (the sum of the sensible and latent heat flux divided by the available energy) across land cover types ranged from 76 to 93%, with a mean value of 84%, and the intercept values ranged from −12.44 to 18.53 $W/m^2$, with a mean value of −1.91 $W/m^2$ (see Figure S2 in supporting information). In general, the surface energy balance closure usually falls in the range from 70 to 90% (Foken et al., 2006; Michel et al., 2016; Twine et al., 2000). Thus, the processed flux data were suitable for model evaluation and optimization.

Furthermore, to make the most of available flux data and to cover as many biomes as possible, we used the flux observations over different periods for cross validation. That is, at each site, 70% of observed data over different periods were used for the optimization process with the remaining data were used for cross validation. In addition, we conducted an additional cross validation using 56 sites for validation and 119 sites for optimization. It was presented in the supporting information as well.

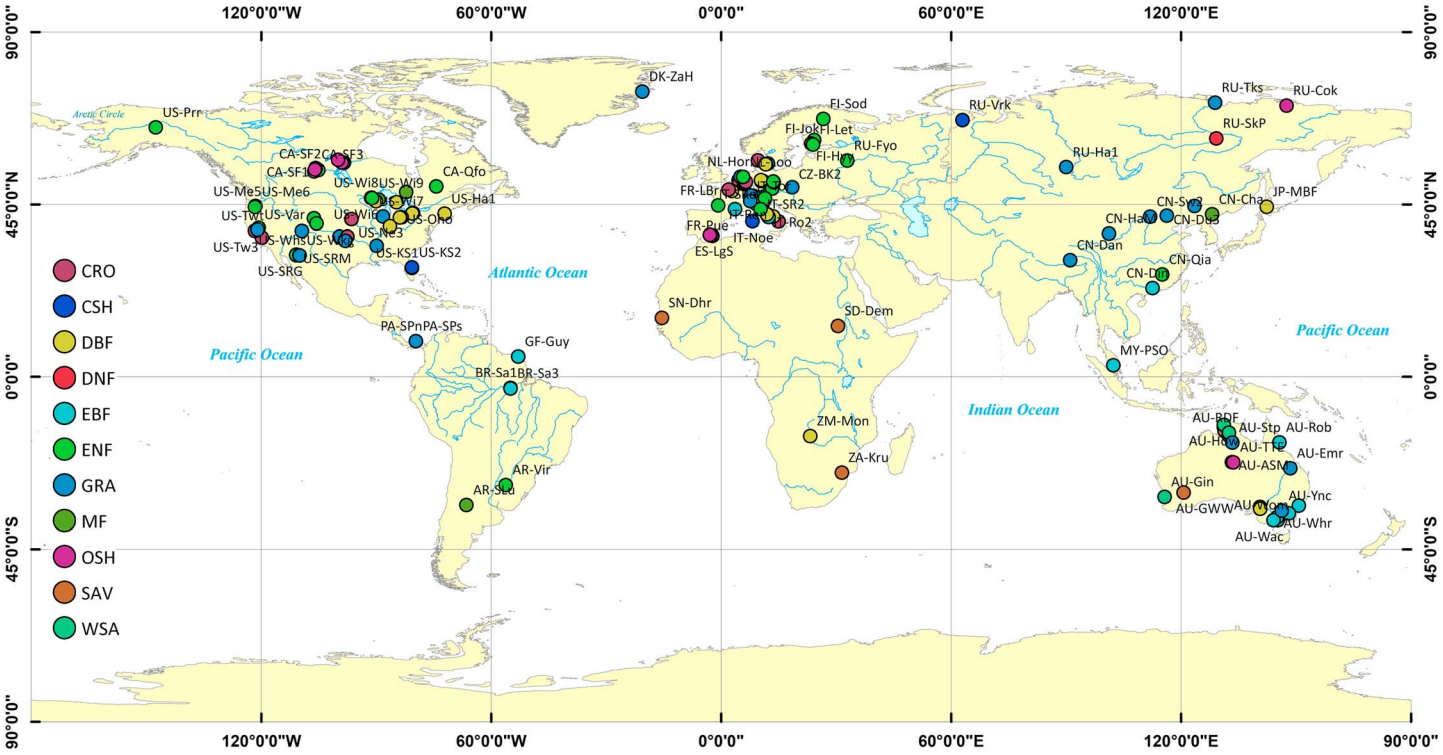


**Figure 2.** Flux sites used in this study. The land cover types are identified based on the International Geosphere-Biosphere Programme biome classification.

#### 3.2.2. Catchment-Scale *E*

We obtained catchment-scale average monthly time series for the water balance components, including precipitation, *E*, streamflow, and the change in water storage, for 32 major (i.e., >200,000 km$^2$) river catchments across the globe (Figure 3) from 1984 to 2006, with the data obtained by Pan et al. (2012). This data set represents an optimal combination of data sources, as it includes in situ observations, remote-sensing observations, land surface model outputs, and reanalysis products and is therefore considered to be the best available water budget data set to date (Li et al., 2013). Here we used the *E* value in the Pan et al. (2012) data set as the observed catchment-scale *E*.

#### 3.2.3. Other Global-Scale *E* Data Sets

To compare the amount and spatial distribution of the optimized *E* data set to those of other related global *E* data sets, we incorporated five widely used data sets into our assessment: (1) the Original MODIS Evapotranspiration product (Mu et al., 2007, 2011), (2) the Global Land Evaporation Amsterdam Model (GLEAM, Miralles et al., 2011; Martens et al., 2017), (3) the Model Tree Ensemble (MTE, Jung et al., 2009, 2011), (4) the PM-Leuning (PML) model (Leuning et al., 2008; Zhang et al., 2008; Zhang, Leuning, et al., 2010), and (5) the European Centre for Medium-range Weather Forecasts Reanalysis-Interim evaporation product (ERA-Interim; Dee et al., 2011). Table 2 summarizes the details of these *E* products.

## 4. Results

### 4.1. Sensitivity Analysis for MOD16

In this study, we used a sample size of 10,000 to calculate the values of the first-order and total-order sensitivities for the key parameters in the MOD16 algorithm. Figures 4a and 4b show the sensitivity indices for the combinations of biomes and parameters. Figures 4c and 4d present the mean values of the first- and total-order SI for each parameter across the biomes, respectively. Overall, the sensitivity values of the eight parameters (except $T_{min\_open}$ and $T_{min\_close}$) varied greatly among the land cover types, and the final outputs were sensitive to all parameters except $T_{min\_open}$ and $T_{min\_close}$ based on a threshold value of 10% for the total-order sensitivity (Tang et al., 2007; Zhang et al., 2013).

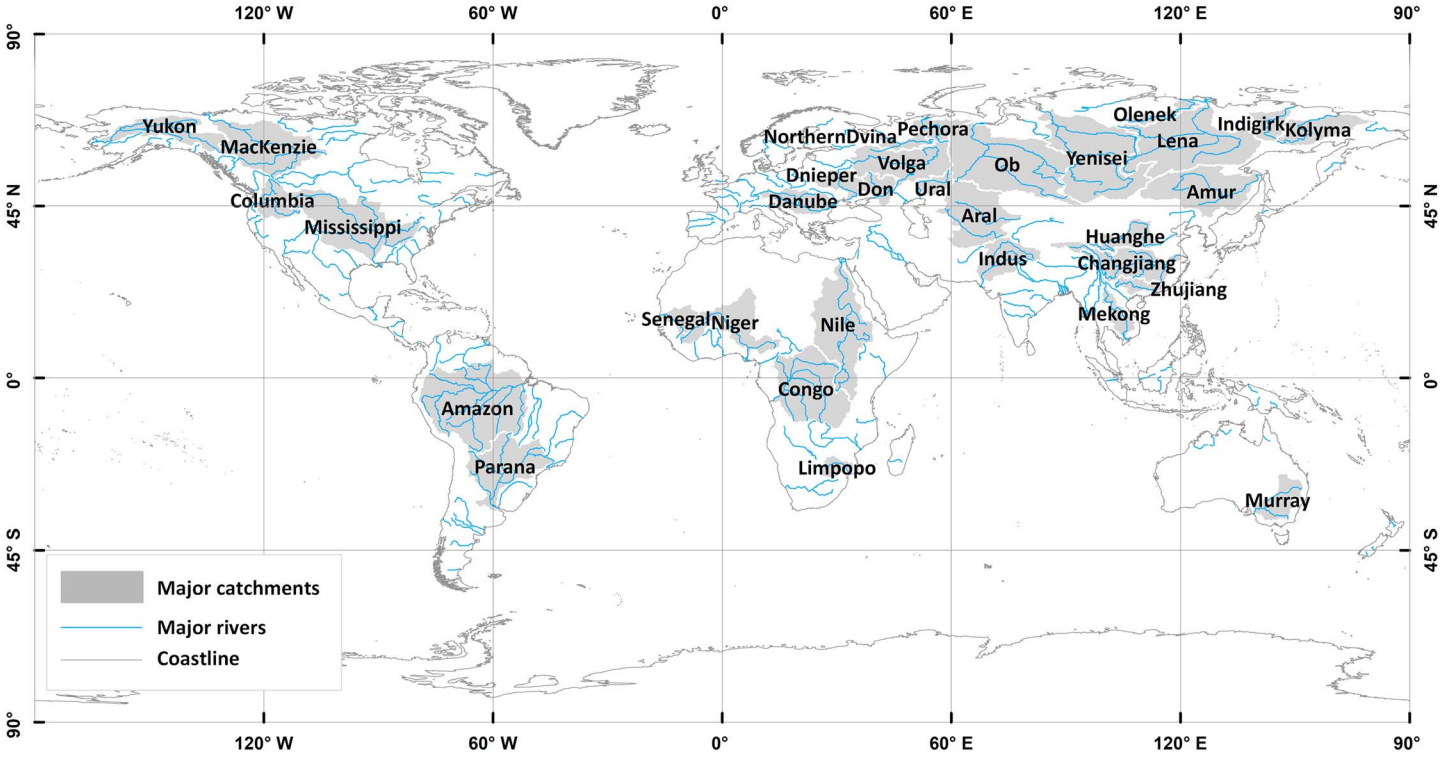


**Figure 3.** The 32 global primary catchments chosen for analysis.

Figures 4a and 4c demonstrate that β has the highest first-order sensitivity (the influence of a single factor on *E*) in MOD16, with values ranging from 10% for MF to 55% for SAV and a mean value of 29%. $rbl_{max}$ and $C_l$ also presented relatively high first-order sensitivity, with values ranging from 2 to 32% and averaging 18% and from 1 to 20% and averaging 10%, respectively. Moreover, the first-order sensitivity of $rbl_{max}$ was even higher than that of β for four biomes (ENF, DNF, MF, and OSH). However, the first-order sensitivity values of $T_{min\_open}$ and $T_{min\_close}$ were near zero for all biomes, indicating that the influence of these parameters on the model outputs was negligible. MOD16 was sensitive to other parameters for specific biomes, even though their first-order sensitivity values were less than about one third of the values for the three parameters to which the model was most sensitive.

Figures 4b and 4d show the total-order sensitivity of the selected parameters, which represents the sensitivity contributed from the parameter itself and from its interactions with other parameters. As in the first-order sensitivity distribution, the model was most sensitive to β, with values ranging from 29% for DBF to 66% for SAV and a mean of 48%. $rbl_{max}$ and $C_l$ again had the second and third largest sensitivities, with values ranging from 11 to 42% and averaging 26% and from 7 to 33% and averaging 17%, respectively. Both are key parameters in soil evaporation and plant transpiration, respectively (Figure 1). The total-order sensitivity

**Table 2**
*Characteristics of the Global Terrestrial E Data Sets Used in the Global-Scale Comparison*

| Data Set | Theoretical basis | Spatial resolution | Temporal resolution | Start date | Version |
|---|---|---|---|---|---|
| MOD16-original | PM equation | 1 km | 8 days | 2000 | 5 |
| GLEAM | PT equation | 0.25° | daily | 1982 | 3.1a |
| PML | PM equation | 0.5° | daily | 1982 | n/a |
| MTE | Model tree | 0.5° | daily | 1982 | n/a |
| ERA-Interim | Reanalysis data | 0.125 to 1° | 3 hr to monthly | 1980 | n/a |

*Note.* n/a means that only a single version existed at the time of our analysis. PM, Penman-Monteith; PT, Priestley-Taylor.

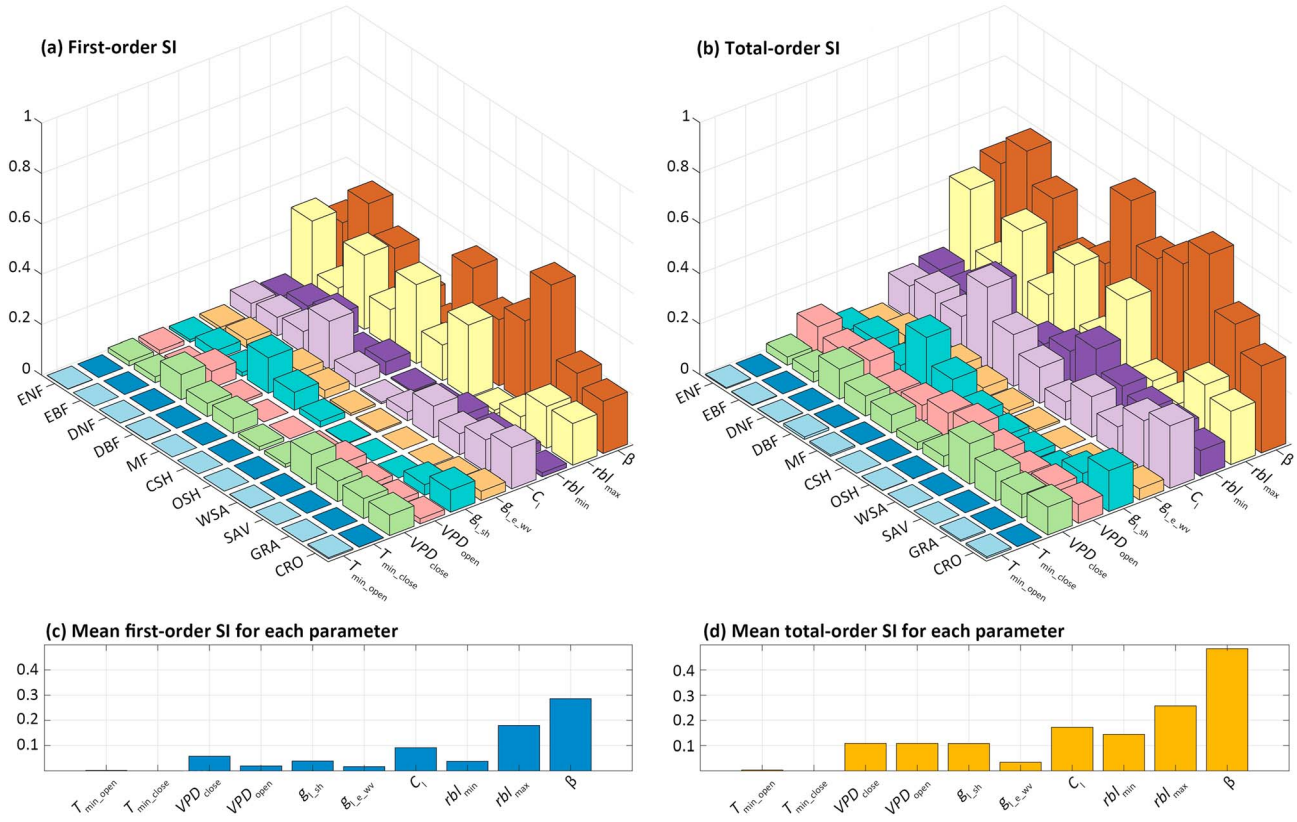


**Figure 4.** Results of the sensitivity analysis in the MOD16 algorithm.

values of other parameters (i.e., $VPD_{close}$, $VPD_{open}$, $g_{l\_sh}$, and $rbl_{min}$) were higher than their first-order sensitivity values, which indicates that the simulated $E$ was influenced by interactions among parameters. Again, MOD16 was insensitive to $T_{min\_open}$ and $T_{min\_close}$ based on the total-order SI for all biomes, with a total sensitivity near zero. Overall, the output of the MOD16 algorithm was sensitive to eight parameters (but especially to β, $rbl_{max}$, and $C_l$) across the biomes.

### 4.2. Parameter Optimization Using Site-Level *E* Observations

Figure 5 shows the medians and 95% credible intervals for the posterior distributions of the eight parameters to which the model was most sensitive. In this figure, the limits of the $x$ axis in each graph represent the range of values in the prior, and the black dots represent the original values for each parameter across different biomes. These results clearly show that the DE-MC method successfully reduced the parameter ranges compared with the assumed prior for most biomes. Among the eight parameters, β, $rbl_{max}$, $C_l$, and $g_{l\_sh}$ showed the greatest variability among the biomes.

For β, the median value ranged between 0.31 for DNF and 0.93 for DBF, and forest ecosystems generally had a high β value (i.e., $\beta > 0.8$, light-green background in Figure 5), whereas nonforest ecosystems (except for GRA and CRO) had a smaller β value (i.e., $\beta < 0.7$, light-yellow background in Figure 5). Nevertheless, these optimized β values for each biome were all higher than the fixed value of 0.2 assumed by the original MOD16. In addition, $C_l$ showed an obvious distinction between the biomes, with much higher median values for CRO, GRA, SAV, and WSA than for the other biomes. The distributions of the optimized $C_l$ values for these biomes were consistent with the original MOD16 distribution reported by Mu et al. (2011), although they decreased at OSH and CSH (approximately 0.002; Table 3).

The posterior distributions of $rbl_{max}$ varied widely among the biomes, and the median values had increased by various degrees (except for EBF and DBF) compared with the original algorithm (Table 3). In contrast, the optimized values of $g_{l\_e\_wv}$ (0.006 to 0.013) were lower in all biomes than the original values (Table 3). For

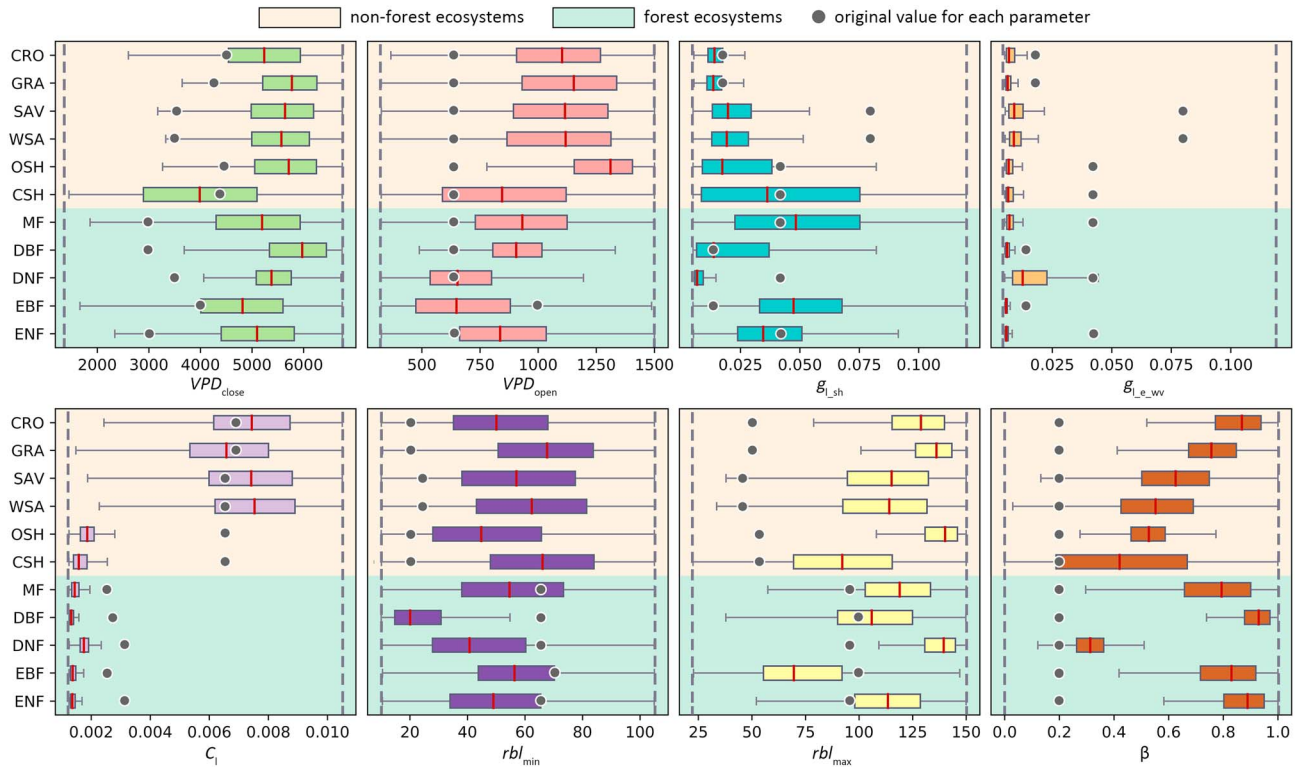


**Figure 5.** Posterior distributions of the eight parameters to which MOD16 was most sensitive for the different biomes. The boxes represent the 95% credible interval, and the vertical line represents the median.

$g_{l\_sh}$, it is interesting to note that the optimized values for the CRO, GRA, SAV, WSA, and OSH biomes (with a relatively low vegetation canopy) were smaller than the values for the other biomes (except DNF and DBF), probably due to the effect of wet canopy evaporation. Furthermore, $VPD_{close}$ and $VPD_{open}$, which are key parameters related to plant transpiration and soil evaporation, had optimized values higher than the original values for most biomes. Finally, $rbl_{min}$ showed a relatively stable posterior distribution across the biomes (with most values between 40 and 70), except for DBF (only 20). The optimized values

**Table 3**
*Comparison of the Original (ori) and Optimized (opt) Values of the MOD16 Parameters*

| | $T_{min\_open}$ (°C) | | $T_{min\_close}$ (°C) | | $VPD_{close}$ (kPa) | | $VPD_{open}$ (kPa) | | $g_{l\_sh}$ ($10^{-2}$ m/s) | | $g_{l\_e\_wv}$ ($10^{-2}$ m/s) | | $C_l$ ($10^{-3}$ m/s) | | $rbl_{min}$ (s/m) | | $rbl_{max}$ (s/m) | | β (kPa) | |
|---|---|---|---|---|---|---|---|---|---|---|---|---|---|---|---|---|---|---|---|---|
| | Ori | Opt | Ori | Opt | Ori | Opt | Ori | Opt | Ori | Opt | Ori | Opt | Ori | Opt | Ori | Opt | Ori | Opt | Ori | Opt |
| ENF | 8.31 | n/a | -8 | n/a | 3.0 | 5.1 | 0.65 | 0.8 | 4 | 3 | 4 | 0.7 | 3.2 | 1.4 | 65 | 50 | 95 | 110 | 0.2 | 0.9 |
| EBF | 9.09 | n/a | -8 | n/a | 4.0 | 4.8 | 1 | 0.7 | 1 | 5 | 1 | 0.6 | 2.5 | 1.4 | 70 | 55 | 100 | 75 | 0.2 | 0.8 |
| DNF | 10.44 | n/a | -8 | n/a | 3.5 | 5.4 | 0.65 | 0.7 | 4 | 1 | 4 | 1.3 | 3.2 | 1.8 | 65 | 40 | 95 | 140 | 0.2 | 0.3 |
| DBF | 9.94 | n/a | −6 | n/a | 2.9 | 6.0 | 0.65 | 0.9 | 1 | 1 | 1 | 0.6 | 2.8 | 1.3 | 65 | 20 | 100 | 100 | 0.2 | 0.9 |
| MF | 9.5 | n/a | −7 | n/a | 2.9 | 5.2 | 0.65 | 0.9 | 4 | 5 | 4 | 0.7 | 2.5 | 1.4 | 65 | 55 | 95 | 120 | 0.2 | 0.8 |
| CSH | 8.61 | n/a | −8 | n/a | 4.3 | 4.0 | 0.65 | 0.8 | 4 | 4 | 4 | 0.6 | 6.5 | 1.7 | 20 | 65 | 55 | 90 | 0.2 | 0.4 |
| OSH | 8.8 | n/a | −8 | n/a | 4.4 | 5.7 | 0.65 | 1.3 | 4 | 2 | 4 | 0.7 | 6.5 | 1.9 | 20 | 45 | 55 | 140 | 0.2 | 0.5 |
| WSA | 11.39 | n/a | −8 | n/a | 3.5 | 5.6 | 0.65 | 1.1 | 8 | 3 | 8 | 0.9 | 6.5 | 7.5 | 25 | 60 | 45 | 115 | 0.2 | 0.5 |
| SAV | 11.39 | n/a | −8 | n/a | 3.6 | 5.6 | 0.65 | 1.1 | 8 | 3 | 8 | 0.9 | 6.5 | 7.4 | 25 | 60 | 45 | 115 | 0.2 | 0.6 |
| GRA | 12.02 | n/a | −8 | n/a | 4.2 | 5.8 | 0.65 | 1.2 | 2 | 1 | 2 | 0.6 | 7 | 6.6 | 20 | 70 | 50 | 135 | 0.2 | 0.8 |
| CRO | 12.02 | n/a | −8 | n/a | 4.5 | 5.2 | 0.65 | 1.1 | 2 | 1 | 2 | 0.7 | 7 | 7.4 | 20 | 50 | 50 | 130 | 0.2 | 0.9 |

*Note.* CSH, closed shrubland; CRO, cropland; DBF, deciduous broadleaf forest; DNF, deciduous needleleaf forest; EBF, evergreen broadleaf forest; ENF, evergreen needleleaf forest; GRA, grassland; MF, mixed forest; OSH, open shrubland; SAV, savanna; WSA, woody savanna.

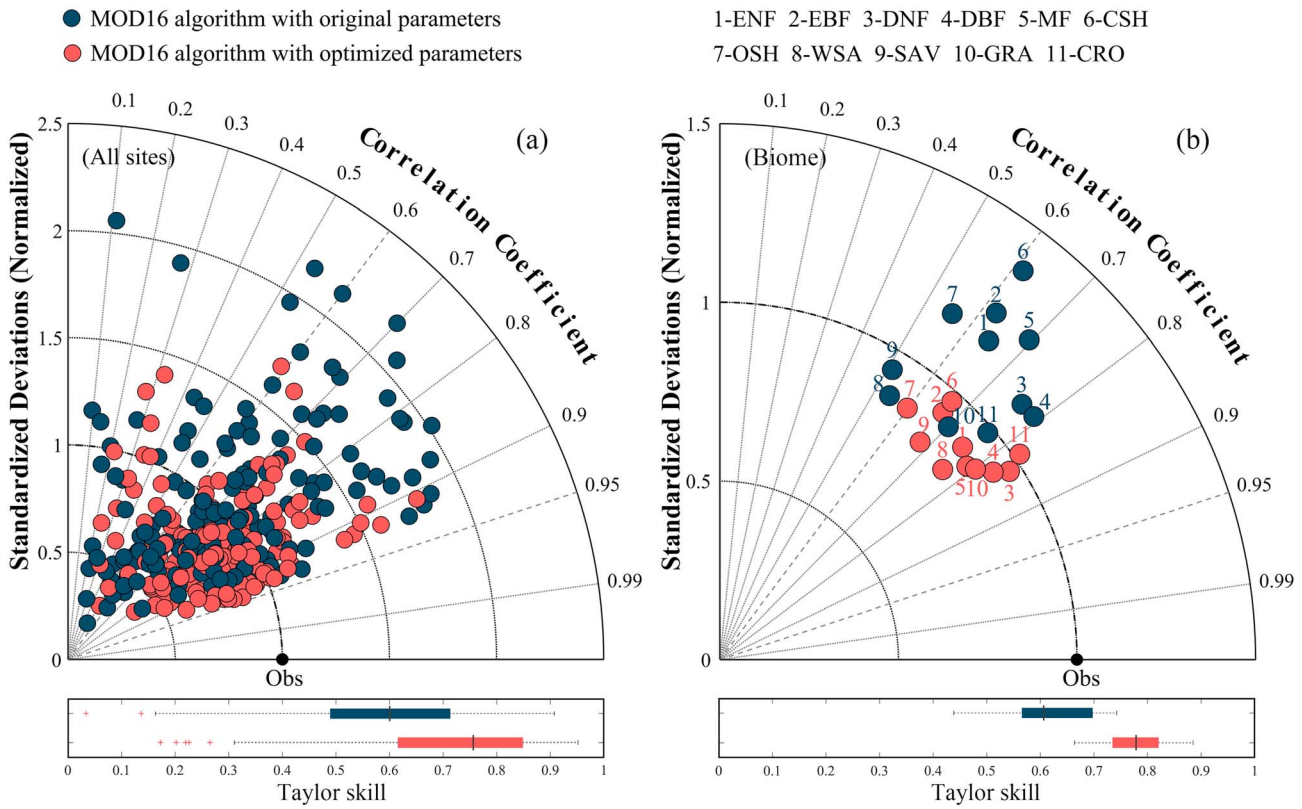


**Figure 6.** Taylor diagram that compares the performance of the MOD16 algorithm using the original and optimized values of the parameters for (a) all sites and (b) individual biomes. The bar charts represent the Taylor skills, the boxes represent the 95% credible interval, and the vertical lines represent the median.

for the biomes with a lower canopy (light-yellow background in Figure 5) were higher than the original MOD16 values (Table 3; Mu et al., 2011).

### 4.3. Evaluation of MOD16 With Optimized Parameters

#### 4.3.1. At Flux Towers

We evaluated the algorithm's performance by comparing its predictions using the optimized and original parameters with the flux data from the FLUXNET sites for all biomes (Figure 6 and Table 4). The Taylor diagrams in Figure 6 compares the model performance, with the two axes representing the normalized standard deviation of the observations ($\sigma_{norm}$), and the curves representing Pearson's correlation coefficient ($r$). At the site level, both the original and optimized MOD16 showed a similar and relatively large range of $r$ values (between 0.10 and 0.95). However, the site-level $\sigma_{norm}$ and Taylor skill (bar graph) of the optimized parameters (red color marks in Figure 6a) are closer to 1 than the original parameters (black color marks in Figure 6a), which indicates that the $E$ value produced by the optimized algorithm agreed better with the observed data.

Figure 6b shows that the algorithm's performance varied for the different biomes. At the biome level, $\sigma_{norm}$ values of the optimized algorithm were closer to 1 than those of the original algorithm, especially for MF, OSH, CSH, ENF, and EBF. Moreover, the correlation coefficients ($r$) for the optimized algorithm (ranging from 0.60 to 0.84), and are slightly higher than those for the original algorithm (ranging from 0.50 to 0.79). Table 4 provides details of the improvement permitted by the optimized model (with the better values boldfaced). As expected, the MOD16 algorithm showed a high degree of biome-specific variation because the parameters to which MOD16 was most sensitive depended heavily on the land cover's attributes. The optimized algorithm often underestimated $E$ (bias < 0), but the magnitude of the difference was much less than that for the original model. Similarly, the optimized algorithm had higher $R^2$ values, lower RE and RMSE values, but greater NSE values (closer to 1) than the original model, which shows greater consistency with the observed $E$ data. In addition, the slope of the regression of the simulated versus actual values was closer to 1 for some biomes using the optimized algorithm, especially in SAV, WSA, GRA, and CRO. Combined

**Table 4**
*Summary Statistics for Performance of the MOD16 Algorithm Using the Original (ori) and Optimized (opt) Parameter Sets*

| | Bias | | $R^2$ | | Slope | | RMSE | | RE | | NSE | |
|---|---|---|---|---|---|---|---|---|---|---|---|---|
| | Ori | Opt | Ori | Opt | Ori | Opt | Ori | Opt | Ori | Opt | Ori | Opt |
| ENF | −0.27 | **0.06** | 0.44 | **0.59** | **0.78** | 0.67 | 1.20 | **0.74** | 0.92 | **0.59** | −0.84 | **0.37** |
| EBF | −0.24 | **0.07** | 0.4 | **0.45** | **0.76** | 0.62 | 1.03 | **0.79** | 0.54 | **0.41** | −0.69 | **0.11** |
| DNF | −0.02 | **0.01** | 0.56 | **0.68** | 0.77 | **0.79** | 0.62 | **0.50** | 0.56 | **0.45** | 0.52 | **0.69** |
| DBF | **−0.07** | −0.18 | 0.62 | **0.67** | **0.84** | 0.78 | 1.15 | **0.96** | 0.70 | **0.60** | 0.02 | **0.33** |
| MF | −0.24 | **−0.04** | 0.49 | **0.61** | **0.94** | 0.73 | 1.10 | **0.60** | 1.04 | **0.56** | −0.27 | **0.59** |
| CSH | −1.54 | **−0.04** | 0.38 | **0.44** | 0.69 | **0.84** | 2.03 | **0.95** | 1.10 | **0.60** | −5.09 | **−0.35** |
| OSH | −0.26 | **0.07** | 0.31 | **0.36** | **0.66** | 0.47 | 0.95 | **0.68** | 1.10 | **0.86** | −1.06 | **−0.15** |
| WSA | 0.33 | **−0.10** | 0.30 | **0.58** | 0.48 | **0.62** | 1.08 | **0.79** | 0.66 | **0.51** | −0.02 | **0.39** |
| SAV | 0.48 | **0.04** | 0.26 | **0.46** | 0.46 | **0.55** | 1.11 | **0.83** | 0.75 | **0.59** | −0.30 | **0.21** |
| GRA | −0.04 | **0.02** | 0.49 | **0.64** | 0.67 | **0.71** | 0.88 | **0.70** | 0.75 | **0.60** | 0.09 | **0.42** |
| CRO | −0.03 | **0.02** | 0.58 | **0.67** | 0.75 | **0.82** | 1.00 | **0.84** | 0.83 | **0.70** | −0.27 | **0.07** |

*Note*. The better value of each pair of values is boldfaced. Statistical indicators: $R^2$, regression goodness of fit; RMSE, root-mean-square error; RE, relative error; NSE, Nash-Sutcliffe efficiency coefficient. CSH, closed shrubland; CRO, cropland; DBF, deciduous broadleaf forest; DNF, deciduous needleleaf forest; EBF, evergreen broadleaf forest; ENF, evergreen needleleaf forest; GRA, grassland; MF, mixed forest; OSH, open shrubland; SAV, savanna; WSA, woody savanna.

with an additional cross validation in Table S2 in the supporting information, in summary, the model with the optimized parameters significantly improved the accuracy of *E* estimates by the MOD16 algorithm at the biome level.

### 4.3.2. At the Catchment and Global Scales

To evaluate the performance of the optimized MOD16 for regional-scale application, we used the long-term water balance *E* (WBE) data for 32 catchments (Figure 3) across a wide range of biomes and climate regimes using data acquired from Pan et al. (2012). We compared the simulated *E* from the optimized and original MOD16 to the WBE data (Figure 7). Figure 7a shows that the slope of the regression of predicted versus actual values for the optimized MOD16 (0.85) was closer to 1 than that of the original MOD16 (0.81). Moreover, its $R^2$ (0.84) was approximately 20% greater than that of the original MOD16 (0.70), indicating that the optimized MOD16 agreed better with the WBE data. In addition, the difference between the optimized and original NSE values for the 32 catchments was generally >0 (i.e., a superior result for the optimized algorithm), indicating that the optimized MOD16 improved *E* estimation for most catchments. Especially in the Amazon, Parana, and Murray catchments, the optimized MOD16 performed much better.

At a global scale, we compared the mean annual *E* value estimated by the original and optimized MOD16 with values from other global terrestrial *E* data sets (i.e., GLEAM, MTE, PML, and ERA-Interim) from 2001 to 2006. The left panel of Figure 8 shows that the overall spatial patterns of each data set were similar

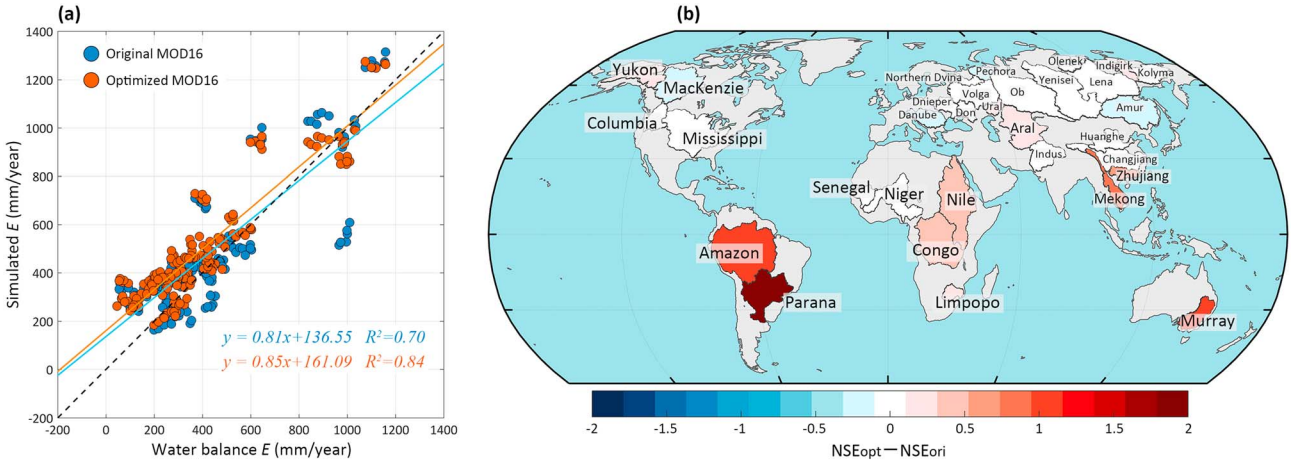


**Figure 7.** Comparison of the original and optimized MOD16 at the catchment scale. (a) Scatterplot for the relationship between the simulated and water-balance *E* values (each point represents one catchment for 1 year). (b) Map of the differences in the Nash-Sutcliffe efficiency coefficient ($NSE_{opt}$-$NSE_{ori}$) for the 32 catchments.

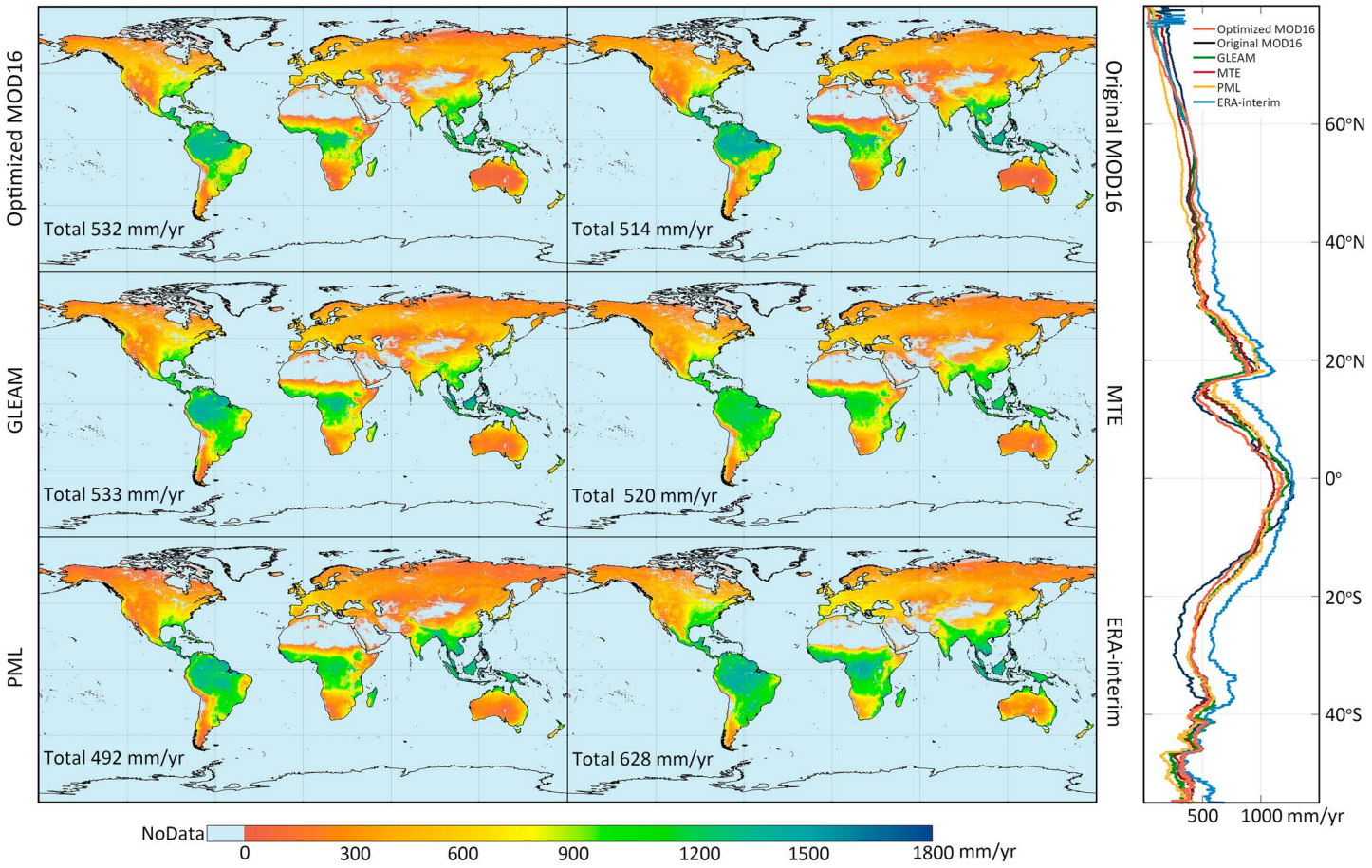


**Figure 8.** Average annual land evapotranspiration from 2001 to 2006 for the optimized MOD16, original MOD16, Global Land Evaporation Amsterdam Model (GLEAM), Model Tree Ensemble (MTE), PM-Leuning (PML), and European Centre for Medium-range Weather Forecasts Reanalysis-Interim evaporation product (ERA-Interim). The latitudinal profiles of these data sets (mean value for a given latitude) are shown in the right panel.

even though the mean annual *E* ranged from 492 to 628 mm/year. The highest mean annual *E* was estimated by ERA-Interim (628 mm/year), and the lowest was obtained from PML (492 mm/year). The optimized MOD16 (532 mm/year) and GLEAM (533 mm/year) algorithms had similar results, and these were slightly higher than the results of the original MOD16 (514 mm/year) and MTE (520 mm/year).

However, some regional differences can be detected among these data sets. For example, the original MOD16 showed lower *E* estimates than the other estimates in southeastern South America. The *E* values for the Indian continent from the PML, MTE, and ERA-Interim were higher than those from the other data sets. The right panel in Figure 8 shows the profiles of latitudinal average *E* for each data set. The *E* profile of ERA-Interim showed clearly higher values than those of the other data sets at most latitudes, and this is consistent with the results of Miralles et al. (2016). Moreover, the *E* profile estimated by the original MOD16 was relatively low in the Southern Hemisphere, between 10 and 40°S; in contrast, the lowest values in the Northern Hemisphere (from 40 to 60°N) were estimated by PML. The optimized MOD16 generally performed similarly to GLEAM and MTE in the *E* profile, except for the latitude ranges from 70 to 80°N and from 10 to 15°N, where it produced lower estimates. Overall, the optimized MOD16 performed reasonably well at regional and global scales.

## 5. Discussion

### 5.1. Analysis of the Parameters of the MOD16 Algorithm

MOD16 is the most widely used algorithm for estimating terrestrial evapotranspiration (Hu et al., 2015; Michel et al., 2016; Miralles et al., 2016). However, apart from the errors associated with the model's

structure and the quality of the forcing data, the model parameters impose considerable uncertainties when using the MOD16 algorithm, particularly for global $E$ applications (Kim et al., 2012; Liu et al., 2013; Ramoelo et al., 2014; Talsma et al., 2018; Yang et al., 2015; Yao et al., 2014). Therefore, to generate a reliable terrestrial $E$ data set, much effort has been devoted to obtaining the optimal parameters for characterizing the heterogeneity of the land surface and vegetation (Bastola et al., 2011; Brigode et al., 2013; McCabe et al., 2016; Zhang et al., 2017). Most of the parameters can only be derived from calibration based on in situ observational data (He et al., 2011). Therefore, identifying the key parameters in the MOD16 algorithm and analyzing their interactions are crucial for further optimization. The present results indicated that the $E$ values were sensitive to 8 of the 10 parameters for all biomes (Figure 4), and these parameters were related to soil and plant canopy constraints.

β, which is set as a constant (0.2 kPa) in the original MOD16 (Mu et al., 2011), was the parameter to which MOD16 was most sensitive across all biomes. The SI values for β were lower for the forest ecosystems than for the other biomes, which is due to the low contribution of soil evaporation to the total $E$ in forest ecosystems. Previous studies have indicated that choosing an appropriate value of β is crucial to accurately estimate soil evaporation (Fisher et al., 2008; García et al., 2013; McCabe et al., 2016; Zhang et al., 2017; Zhu et al., 2016). After testing the effects of different β values on soil evaporation, Yang et al. (2015) set β to 1 (kPa) to estimate $E$ over the oasis region of northwestern China. For an environment with limited soil moisture, a lower β value (e.g., 0.1 kPa) has been proposed and may provide a more meaningful estimate of $E$ (García et al., 2013; McCabe et al., 2016; Zhang et al., 2017; Zhu et al., 2014). Figure 5 shows that the optimized median values of β ranged from 0.31 to 0.93 kPa across the different biomes and that these values were all greater than the β value (0.2 kPa) used in the original algorithm. Furthermore, relatively high values of β (approximately 0.8 kPa) were found in the forest, cropland, and grassland biomes, versus lower values (<0.6 kPa) occurred in the biomes with low vegetation cover and dry environmental conditions (i.e., SAV, WAS, OSH, and CSH), which lead to low soil evaporation due to the constraint of soil moisture stress.

$C_l$ was another parameter to which MOD16 was sensitive (Figure 4). It represents the mean potential stomatal conductance per unit leaf area. This is important because leaf stomatal conductance dominates a plant's transpiration process and responds rapidly to changes in environmental conditions such as the air temperature, relative humidity, and soil water content (Bai et al., 2015; Leuning et al., 2008; Zhang, Leuning, et al., 2010). Besides, the bias of MOD16 is likely related to the scaling stomatal conductance of canopy transpiration (Talsma et al., 2018). Hence, an optimal value of $C_l$ could improve characterization of the transpiration mechanisms in different biomes and significantly improve estimates of the plant transpiration rate (Ershadi et al., 2015; Zhu et al., 2014). Due to the high proportion of plant transpiration over the diverse biomes, the sensitivity values of $C_l$ for the biomes with good vegetation cover (i.e., forests, cropland, and grassland) were higher than for those with sparse vegetation cover (i.e., savanna and shrubland; Figure 4). Overall, the optimized values of $C_l$ for most biomes were similar to those in the original algorithm. However, the optimized $C_l$ values for the OSH and CSH (~0.0018) were slightly lower than the original values (0.0065), and were closer to the maximum stomatal conductance for open shrubland (0.0028; Leuning et al., 2008; Zhang et al., 2008).

The process of soil evaporation is linked both with soil physical properties (such as soil moisture, pore diameter, and texture) and with the air turbulence at the boundary between the soil and atmosphere (van de Griend & Owe, 1994). Nevertheless, to reduce the quantity of forcing data and make the algorithm more applicable at a global scale, MOD16 employed several semiempirical parameters to characterize soil evaporation. For an algorithm based on a PM equation, the proper parameterization of surface resistance significantly influences the accuracy of the simulated $E$ (Ershadi et al., 2015; Zhang et al., 2008). In MOD16, the simulated $E$ was sensitive to four soil-resistance-related parameters ($rbl_{max}$, $rbl_{min}$, $VPD_{close}$, and $VPD_{open}$) for all biomes (Figure 4). As expected, these parameters showed high biome-specific variation across the different environments. However, the optimized values of these four parameters were generally higher than their original values for each biome (Figure 5), which can result in strong constraints on the soil evaporation processes.

Furthermore, the wet canopy evaporation ($E_{wet}$), which relates to evaporation from precipitation intercepted by the plant canopy, has normally been regarded as a significant component of the total evapotranspiration, especially in tropical rainforests (Herbst et al., 2008; Jiménez et al., 2011). Previous studies developed models

for estimating the interception evaporation, such as the analytical model of Gash (1979), which needs daily precipitation data and site parameters to characterize the water balance of the wet canopy. However, the MOD16 algorithm does not use rainfall data. Instead, MOD16 calculates $E_{wet}$ based on the PM equation and employs two parameters ($g_{l\_sh}$ and $g_{l\_e\_wv}$) related to the surface and aerodynamic resistance of the wet canopy. Previous studies indicated that the proportion and magnitude of the interception evaporation from MOD16 were much higher than in other global $E$ products (i.e., GLEAM and PT-JPL; Miralles et al., 2016). As shown in Table 3 and Figure 5, the optimized values of $g_{l\_e\_wv}$ were substantially lower than the original values for all biomes. This indicates that the surface resistance of the wet canopy will become much stronger than that in the original algorithm and that this will therefore reduce the simulated $E_{wet}$. In addition, the optimized $g_{l\_sh}$ had larger values for some forest biomes (especially EBF) than for other biomes with low canopy heights. This will result in a lower aerodynamic resistance in the forest biomes, which is probably due to the interaction between the relative humidity and the low roughness of the canopy surface.

### 5.2. Evaluation of the Optimized Algorithm at Site, Catchment, and Global Scales

At the site scale, the optimized MOD16 reliably simulated $E$, with a lower bias, RMSE, and RE and a higher NSE than the original MOD16 (Figure 6 and Table 4). The original MOD16 tended to underestimate $E$ for most biomes (Table 4), which was consistent with previous studies (Long et al., 2014; Vinukollu et al., 2011; Yang et al., 2015; Yao et al., 2014). It should be noted that differences between the observed and simulated results using the optimized parameters were largest in the OSH, CSH, SAV, CRO, and EBF biomes, which might be attributable to structural errors in the algorithm. The MOD16 uses micrometeorological variables (i.e., air temperature and VPD) to characterize the effects of water limitation on soil evaporation and plant transpiration processes, which is based on the assumption of a strong link between soil moisture and evaporative demand of the adjacent atmosphere (Seneviratne et al., 2010). However, this assumption is only valid over large spatial and temporal scales when the vertically adjacent atmosphere is in equilibrium with the underlying soil (Fisher et al., 2008; Long & Singh, 2010; Morillas et al., 2013; Vinukollu, Wood, et al., 2011; Yang et al., 2015). Nevertheless, the definition of the wet fraction of evaporation ($f_{wet}$) in MOD16 was simplified as a semiempirical function associated with relative humidity ($RH$), which depends more strongly on the volume and duration of the precipitation (Miralles et al., 2011; Shuttleworth & Calder, 1979) and on vegetation properties (e.g., broad leaves can intercept more rainfall than needle leaves). Hence, continuous efforts should be devoted to understanding the mechanisms that underlie evapotranspiration, since a more accurate parameterization scheme would improve the accuracy of the MOD16 algorithm.

The catchment water-balance $E$ data provide another way to validate the simulated $E$ (Sheffield et al., 2009). Figure 7 shows that the optimized MOD16 provided a better fit to the data (i.e., the slope, $R^2$, and NSE) for the 32 major basins that we analyzed. Zhang, Kimball, et al., 2010 evaluated a satellite-derived global $E$ data set of major global catchments and obtained $R^2 = 0.80$ and RMSE = 186.3 mm/year, which are similar to the optimized MOD16 results. Jung et al. (2010) compared the mean annual MTE model data with the mean annual $E$ from catchment water-balance data and obtained $R^2 = 0.92$. This is due to the MTE data being upscaled from the observed flux data, which is more consistent with the precipitation and discharge data used in the derivation of the catchment water balance. Note that the optimized MOD16 greatly improved the algorithm's performance for the catchments in South America, Africa, Southeast Asia, and Oceania, where the original MOD16 was generally inconsistent with the $E$ based on in situ observations (Michel et al., 2016; Ramoelo et al., 2014) and other simulations (Miralles et al., 2016).

At a global scale, the optimized MOD16 showed better spatial agreement with the other products (i.e., GLEAM, MTE, and PML) than the original MOD16, especially in the southern hemisphere (Figure 8). Previous studies have indicated that the original MOD16 products tended to underestimate $E$ in the southern hemisphere and overestimate $E$ at high latitudes in the northern hemisphere (e.g., Miralles et al., 2016). Furthermore, the original MOD16 performed less well over sparsely vegetated areas in the central Great Plains area of the United States (Velpuri et al., 2013), as well as in the Sahel, Southern Africa, and arid Mediterranean regions (Trambauer et al., 2014). In contrast, the optimized MOD16 improved the performance of the simulation in these regions and agreed better with the GLEAM and MTE data sets. This shows that the optimized parameters successfully reduced the error caused by the original parameterization scheme. In addition, the mean annual terrestrial $E$ from 2001 to 2006 for the optimized MOD16 was 532 mm/year, which was higher than that estimated by the original MOD16 (514 mm/year) and much

closer to that estimated by GLEAM (533 mm/year). Mueller et al. (2013) calculated the mean annual terrestrial $E$ (550 mm/year) based on merged synthesis products. In addition, it is important to note that the differences in the algorithm structure and uncertainties in the forcing data cause large inter–data set differences. For example, the latitudinal profile of MTE exhibited the lowest values near the equator, which might be associated with the lack of interception evaporation in the eddy covariance measurements (Miralles et al., 2016; van Dijk et al., 2015). Nevertheless, the multiple data sets provided a reference range for the latitudinal average of terrestrial $E$.

## 6. Conclusions

Understanding the influence of the parameterization scheme is nontrivial in a PM-type evaporation algorithm. In the present study, we applied the Sobol' method to identify the key parameters in the MOD16 algorithm. We found that the simulated $E$ was most sensitive to eight parameters ($\beta$, $C_l$, $rbl_{max}$, $rbl_{min}$, $g_{l\_sh}$, $g_{l\_e\_wv}$, $VPD_{close}$, and $VPD_{open}$) under different environmental conditions. Most of these key parameters were associated with the resistance parameterizations, which significantly influenced the accuracy of the simulation. It should be noted that MOD16 exhibited the highest sensitivity to $\beta$ for all biomes, whereas $\beta$ was considered to be a constant in the original MOD16. We optimized the eight parameters to which MOD16 was most sensitive by using the DE-MC method based on data from 175 flux sites. The resulting posterior distributions of the selected parameters were successfully constrained by these observations (i.e., showed a narrower range of variation than the original MOD16). We evaluated the resulting MOD16 algorithm with optimized parameters at multiple spatial scales, including a cross validation with in situ eddy covariance data and comparisons with WBE data at 32 catchments and other terrestrial $E$ products at global scale. The optimized algorithm performed better than the original algorithm in most cases.

Nonetheless, deficiencies remain in the MOD16 algorithm for some specific cases even after optimization. This may relate to errors associated with the algorithm's structure and uncertainties in the forcing data. The mechanisms that underlie $E$ not only require separate analysis of the components (e.g., interception, soil evaporation, and plant transpiration) because of their different biophysical drivers but also require comprehensive consideration of the continuous transfers of water through the soil-plant-atmosphere-continuum. The characterization of soil moisture is inadequate in the MOD16 algorithm, in part because it is a significant challenge to generate suitable soil moisture data for a global $E$ data set with high spatiotemporal resolution. Furthermore, the energy partitioning scheme creates a large range of uncertainty for the different components of $E$, which are difficult to validate separately because conventional technologies (e.g., eddy covariance, scintillometers, and lysimeters) cannot distinguish the components of the total evapotranspiration. In addition, with increasing amounts of in situ flux data and other available observation data, further optimization of the parameters of the MOD16 algorithm should be conducted to further improve the accuracy of its simulation.

**Acknowledgments**
This work is funded by the National Key R&D Program of China (2018YFC0406602), the National Natural Science Foundation of China (grants 41871078 and 41571016). We are grateful to the principal investigators and their teams of all the data set used in this study. The flux data from FLUXNET are available at https://fluxnet.fluxdata.org. The meteorological data from MERRA-2 are available at https://disc.sci.gsfc.nasa.gov. The MODIS products used in this study are available at https://lpdaac.usgs.gov/. GLEAM data sets are available at https://www.gleam.eu/. PML data sets are available at https://data.csiro.au. ERA-Interim data sets are available at https://www.ecmwf.int/. All generated data and methods used in this study can be downloaded from https://github.com/kunlz/MOD16_Supporting_Data. We would like to thank Peter A. Troch (Editor), the Associate Editor, and the two anonymous reviewers for their critical reviews and constructive comments. The authors declare no conflict of interest.

## References

Bai, Y., Zhu, G., Su, Y., Zhang, K., Han, T., Ma, J., et al. (2015). Hysteresis loops between canopy conductance of grapevines and meteorological variables in an oasis ecosystem. *Agricultural and Forest Meteorology*, *214-215*, 319–327. https://doi.org/10.1016/j.agrformet.2015.08.267

Baldocchi, D., Falge, E., Gu, L., Olson, R., Hollinger, D., Running, S., et al. (2001). FLUXNET: A new tool to study the temporal and spatial variability of ecosystem–scale carbon dioxide, water vapor, and energy flux densities. *Bulletin of the American Meteorological Society*, *82*(11), 2415–2434. https://doi.org/10.1175/1520-0477(2001)082<2415:FANTTS>2.3.CO;2

Bastiaanssen, W. G. M., Pelgrum, H., Wang, J., Ma, Y., Moreno, J. F., Roerink, G. J., & van der Wal, T. (1998). A remote sensing surface energy balance algorithm for land (SEBAL): Part 2: Validation. *Journal of Hydrology*, *212–213*, 213–229. https://doi.org/10.1016/S0022-1694(98)00254-6

Bastola, S., Murphy, C., & Sweeney, J. (2011). The role of hydrological modelling uncertainties in climate change impact assessments of Irish river catchments. *Advances in Water Resources*, *34*(5), 562–576. https://doi.org/10.1016/j.advwatres.2011.01.008

Bouchet, R. J. (1963). Evapotranspiration réelle et potentielle, signification climatique. *IAHS Publ*, *62*, 134–142.

Bouda, M., Rousseau, A. N., Gumiere, S. J., Gagnon, P., Konan, B., & Moussa, R. (2014). Implementation of an automatic calibration procedure for HYDROTEL based on prior OAT sensitivity and complementary identifiability analysis. *Hydrological Processes*, *28*(12), 3947–3961. https://doi.org/10.1002/hyp.9882

Braswell, B. H., Sacks, W. J., Linder, E., & Schimel, D. S. (2005). Estimating diurnal to annual ecosystem parameters by synthesis of a carbon flux model with eddy covariance net ecosystem exchange observations. *Global Change Biology*, *11*(2), 335–355. https://doi.org/10.1111/j.1365-2486.2005.00897.x

Brigode, P., Oudin, L., & Perrin, C. (2013). Hydrological model parameter instability: A source of additional uncertainty in estimating the hydrological impacts of climate change? *Journal of Hydrology*, *476*, 410–425. https://doi.org/10.1016/j.jhydrol.2012.11.012

Chen, Y., Xia, J., Liang, S., Feng, J., Fisher, J. B., Li, X., et al. (2014). Comparison of satellite-based evapotranspiration models over terrestrial ecosystems in China. *Remote Sensing of Environment*, *140*, 279–293. https://doi.org/10.1016/j.rse.2013.08.045

Clark, J. S., & Gelfand, A. E. (2006). A future for models and data in environmental science. *Trends in Ecology & Evolution*, *21*(7), 375–380. https://doi.org/10.1016/j.tree.2006.03.016

Cleugh, H. A., Leuning, R., Mu, Q., & Running, S. W. (2007). Regional evaporation estimates from flux tower and MODIS satellite data. *Remote Sensing of Environment*, *106*(3), 285–304. https://doi.org/10.1016/j.rse.2006.07.007

Confalonieri, R., Bellocchi, G., Tarantola, S., Acutis, M., Donatelli, M., & Genovese, G. (2010). Sensitivity analysis of the rice model WARM in Europe: Exploring the effects of different locations, climates and methods of analysis on model sensitivity to crop parameters. *Environmental Modelling & Software*, *25*(4), 479–488. https://doi.org/10.1016/j.envsoft.2009.10.005

Dee, D. P., Uppala, S. M., Simmons, A. J., Berrisford, P., Poli, P., Kobayashi, S., et al. (2011). The ERA-Interim reanalysis: Configuration and performance of the data assimilation system. *Quarterly Journal of the Royal Meteorological Society*, *137*(656), 553–597. https://doi.org/10.1002/qj.828

Ershadi, A., McCabe, M. F., Evans, J. P., Chaney, N. W., & Wood, E. F. (2014). Multi-site evaluation of terrestrial evaporation models using FLUXNET data. *Agricultural and Forest Meteorology*, *187*, 46–61. https://doi.org/10.1016/j.agrformet.2013.11.008

Ershadi, A., McCabe, M. F., Evans, J. P., & Wood, E. F. (2015). Impact of model structure and parameterization on Penman–Monteith type evaporation models. *Journal of Hydrology*, *525*, 521–535. https://doi.org/10.1016/j.jhydrol.2015.04.008

Fisher, J. B., Tu, K. P., & Baldocchi, D. D. (2008). Global estimates of the land–atmosphere water flux based on monthly AVHRR and ISLSCP-II data, validated at 16 FLUXNET sites. *Remote Sensing of Environment*, *112*(3), 901–919. https://doi.org/10.1016/j.rse.2007.06.025

Foken, T., Wimmer, F., Mauder, M., Thomas, C., & Liebethal, C. (2006). Some aspects of the energy balance closure problem. *Atmospheric Chemistry & Physics*, *6*(12), 4395–4402. https://doi.org/10.5194/acp-6-4395-2006

Foscarini, F., Bellocchi, G., Confalonieri, R., Savini, C., & Van den Eede, G. (2010). Sensitivity analysis in fuzzy systems: Integration of SimLab and DANA. *Environmental Modelling & Software*, *25*(10), 1256–1260. https://doi.org/10.1016/j.envsoft.2010.03.024

García, M., Sandholt, I., Ceccato, P., Ridler, M., Mougin, E., Kergoat, L., et al. (2013). Actual evapotranspiration in drylands derived from in-situ and satellite data: Assessing biophysical constraints. *Remote Sensing of Environment*, *131*, 103–118. https://doi.org/10.1016/j.rse.2012.12.016

Gash, J. H. C. (1979). An analytical model of rainfall interception by forests. *Quarterly Journal of the Royal Meteorological Society*, *105*(443), 43–55. https://doi.org/10.1002/qj.49710544304

Gelaro, R., Mccarty, W., Suárez, M. J., Todling, R., Molod, A., Takacs, L., et al. (2017). The Modern-Era Retrospective Analysis for Research and Applications, Version 2 (MERRA-2). *Journal of Climate*, *30*(14), 5419–5454. https://doi.org/10.1175/JCLI-D-16-0758.1

Haario, H., Laine, M., Mira, A., & Saksman, E. (2006). DRAM: Efficient adaptive MCMC. *Statistics and Computing*, *16*(4), 339–354. https://doi.org/10.1007/s11222-006-9438-0

He, M., Hogue, T. S., Franz, K. J., Margulis, S. A., & Vrugt, J. A. (2011). Corruption of parameter behavior and regionalization by model and forcing data errors: A Bayesian example using the SNOW17 model. *Water Resources Research*, *47*, W01403. https://doi.org/10.1029/2010WR009753

Herbst, M., Rosier, P. T. W., McNeil, D. D., Harding, R. J., & Gowing, D. J. (2008). Seasonal variability of interception evaporation from the canopy of a mixed deciduous forest. *Agricultural and Forest Meteorology*, *148*(11), 1655–1667. https://doi.org/10.1016/j.agrformet.2008.05.011

Hu, G., Jia, L., & Menenti, M. (2015). Comparison of MOD16 and LSA-SAF MSG evapotranspiration products over Europe for 2011. *Remote Sensing of Environment*, *156*, 510–526. https://doi.org/10.1016/j.rse.2014.10.017

Huisman, J. A., Rings, J., Vrugt, J. A., Sorg, J., & Vereecken, H. (2010). Hydraulic properties of a model dike from coupled Bayesian and multi-criteria hydrogeophysical inversion. *Journal of Hydrology*, *380*(1-2), 62–73. https://doi.org/10.1016/j.jhydrol.2009.10.023

Jiang, L., & Islam, S. (1999). A methodology for estimation of surface evapotranspiration over large areas using remote sensing observations. *Geophysical Research Letters*, *26*(17), 2773–2776. https://doi.org/10.1029/1999GL006049

Jiménez, C., Prigent, C., Mueller, B., Seneviratne, S. I., McCabe, M. F., Wood, E. F., et al. (2011). Global intercomparison of 12 land surface heat flux estimates. *Journal of Geophysical Research*, *116*, D02102. https://doi.org/10.1029/2010JD014545

Jung, M., Reichstein, M., & Bondeau, A. (2009). Towards global empirical upscaling of FLUXNET eddy covariance observations: Validation of a model tree ensemble approach using a biosphere model. *Biogeosciences*, *6*(10), 2001–2013. https://doi.org/10.5194/bg-6-2001-2009

Jung, M., Reichstein, M., Ciais, P., Seneviratne, S. I., Sheffield, J., Goulden, M. L., et al. (2010). Recent decline in the global land evapotranspiration trend due to limited moisture supply. *Nature*, *467*(7318), 951–954. https://doi.org/10.1038/nature09396

Jung, M., Reichstein, M., Margolis, H. A., Cescatti, A., Richardson, A. D., Arain, M. A., et al. (2011). Global patterns of land-atmosphere fluxes of carbon dioxide, latent heat, and sensible heat derived from eddy covariance, satellite, and meteorological observations. *Journal of Geophysical Research*, *116*, G00J07. https://doi.org/10.1029/2010JG001566

Keating, E. H., Doherty, J., Vrugt, J. A., & Kang, Q. (2010). Optimization and uncertainty assessment of strongly nonlinear groundwater models with high parameter dimensionality. *Water Resources Research*, *46*, W10517. https://doi.org/10.1029/2009WR008584

Kim, H. W., Hwang, K., Mu, Q., Lee, S. O., & Choi, M. (2012). Validation of MODIS 16 global terrestrial evapotranspiration products in various climates and land cover types in Asia. *KSCE Journal of Civil Engineering*, *16*(2), 229–238. https://doi.org/10.1007/s12205-012-0006-1

Legates, D. R., & McCabe, G. J. (1999). Evaluating the use of "goodness-of-fit" measures in hydrologic and hydroclimatic model validation. *Water Resources Research*, *35*(1), 233–241. https://doi.org/10.1029/1998WR900018

Leuning, R., Zhang, Y. Q., Rajaud, A., Cleugh, H., & Tu, K. (2008). A simple surface conductance model to estimate regional evaporation using MODIS leaf area index and the Penman-Monteith equation. *Water Resources Research*, *44*, W10419. https://doi.org/10.1029/2007WR006562

Li, D., Pan, M., Cong, Z., Zhang, L., & Wood, E. (2013). Vegetation control on water and energy balance within the Budyko framework. *Water Resources Research*, *49*, 969–976. https://doi.org/10.1002/wrcr.20107

Liu, S. M., Xu, Z. W., Zhu, Z. L., Jia, Z. Z., & Zhu, M. J. (2013). Measurements of evapotranspiration from eddy-covariance systems and large aperture scintillometers in the Hai River Basin, China. *Journal of Hydrology*, *487*, 24–38. https://doi.org/10.1016/j.jhydrol.2013.02.025

Long, D., Longuevergne, L., & Scanlon, B. R. (2014). Uncertainty in evapotranspiration from land surface modeling, remote sensing, and GRACE satellites. *Water Resources Research*, *50*, 1131–1151. https://doi.org/10.1002/2013WR014581

Long, D., & Singh, V. P. (2010). Integration of the GG model with SEBAL to produce time series of evapotranspiration of high spatial resolution at watershed scales. *Journal of Geophysical Research*, *115*, D21128. https://doi.org/10.1029/2010JD014092

Long, D., & Singh, V. P. (2012). A Two-source Trapezoid Model for Evapotranspiration (TTME) from satellite imagery. *Remote Sensing of Environment*, *121*, 370–388. https://doi.org/10.1016/j.rse.2012.02.015

Martens, B., Miralles, D. G., Lievens, H., van der Schalie, R., de Jeu, R. A. M., Fernández-Prieto, D., et al. (2017). GLEAM v3: Satellite-based land evaporation and root-zone soil moisture. *Geoscientific Model Development*, *10*(5), 1903–1925. https://doi.org/10.5194/gmd-10-1903-2017

McCabe, M. F., Ershadi, A., Jimenez, C., Miralles, D. G., Michel, D., & Wood, E. F. (2016). The GEWEX LandFlux project: Evaluation of model evaporation using tower-based and globally gridded forcing data. *Geoscientific Model Development*, *9*(1), 283–305. https://doi.org/10.5194/gmd-9-283-2016

Michel, C., Andréassian, V., & Perrin, C. (2005). Soil conservation service curve number method: How to mend a wrong soil moisture accounting procedure? *Water Resources Research*, *41*, W02011. https://doi.org/10.1029/2004WR003191

Michel, D., Jiménez, C., Miralles, D. G., Jung, M., Hirschi, M., Ershadi, A., et al. (2016). The WACMOS-ET project—Part 1: Tower-scale evaluation of four remote-sensing-based evapotranspiration algorithms. *Hydrology and Earth System Sciences*, *20*(2), 803–822. https://doi.org/10.5194/hess-20-803-2016

Miralles, D. G., De Jeu, R. A. M., Gash, J. H., Holmes, T. R. H., & Dolman, A. J. (2011). Magnitude and variability of land evaporation and its components at the global scale. *Hydrology and Earth System Sciences*, *15*(3), 967–981. https://doi.org/10.5194/hess-15-967-2011

Miralles, D. G., Jiménez, C., Jung, M., Michel, D., Ershadi, A., McCabe, M. F., et al. (2016). The WACMOS-ET project—Part 2: Evaluation of global terrestrial evaporation data sets. *Hydrology and Earth System Sciences*, *20*(2), 823–842. https://doi.org/10.5194/hess-20-823-2016

Morillas, L., Leuning, R., Villagarcía, L., García, M., Serrano-Ortiz, P., & Domingo, F. (2013). Improving evapotranspiration estimates in Mediterranean drylands: The role of soil evaporation: Evapotranspiration estimation in Mediterranean dry lands. *Water Resources Research*, *49*, 6572–6586. https://doi.org/10.1002/wrcr.20468

Mu, Q., Heinsch, F. A., Zhao, M., & Running, S. W. (2007). Development of a global evapotranspiration algorithm based on MODIS and global meteorology data. *Remote Sensing of Environment*, *111*(4), 519–536. https://doi.org/10.1016/j.rse.2007.04.015

Mu, Q., Zhao, M., & Running, S. W. (2011). Improvements to a MODIS global terrestrial evapotranspiration algorithm. *Remote Sensing of Environment*, *115*(8), 1781–1800. https://doi.org/10.1016/j.rse.2011.02.019

Mueller, B., Hirschi, M., Jimenez, C., Ciais, P., Dirmeyer, P. A., Dolman, A. J., et al. (2013). Benchmark products for land evapotranspiration: LandFlux-EVAL multi-data set synthesis. *Hydrology and Earth System Sciences*, *17*(10), 3707–3720. https://doi.org/10.5194/hess-17-3707-2013

Nash, J. E., & Sutcliffe, J. V. (1970). River flow forecasting through conceptual models. Part I—A discussion of principles. *Journal of Hydrology*, *10*(3), 282–290. https://doi.org/10.1016/0022-1694(70)90255-6

Norman, J. M., Kustas, W. P., & Humes, K. S. (1995). Source approach for estimating soil and vegetation energy fluxes in observations of directional radiometric surface temperature. *Agricultural and Forest Meteorology*, *77*(3-4), 263–293. https://doi.org/10.1016/0168-1923(95)02265-Y

Nossent, J., Elsen, P., & Bauwens, W. (2011). Sobol' sensitivity analysis of a complex environmental model. *Environmental Modelling & Software*, *26*(12), 1515–1525. https://doi.org/10.1016/j.envsoft.2011.08.010

Oki, T., & Kanae, S. (2006). Global hydrological cycles and world water resources. *Science*, *313*(5790), 1068–1072. https://doi.org/10.1126/science.1128845

Pan, M., Sahoo, A. K., Troy, T. J., Vinukollu, R. K., Sheffield, J., & Wood, E. F. (2012). Multisource estimation of long-term terrestrial water budget for major global river basins. *Journal of Climate*, *25*(9), 3191–3206. https://doi.org/10.1175/JCLI-D-11-00300.1

Pappenberger, F., Beven, K. J., Ratto, M., & Matgen, P. (2008). Multi-method global sensitivity analysis of flood inundation models. *Advances in Water Resources*, *31*(1), 1–14. https://doi.org/10.1016/j.advwatres.2007.04.009

Ramoelo, A., Majozi, N., Mathieu, R., Jovanovic, N., Nickless, A., & Dzikiti, S. (2014). Validation of global evapotranspiration product (MOD16) using flux tower data in the African savanna, South Africa. *Remote Sensing*, *6*(8), 7406–7423. https://doi.org/10.3390/rs6087406

Ryu, Y., Baldocchi, D. D., Black, T. A., Detto, M., Law, B. E., Leuning, R., et al. (2012). On the temporal upscaling of evapotranspiration from instantaneous remote sensing measurements to 8-day mean daily-sums. *Agricultural and Forest Meteorology*, *152*, 212–222. https://doi.org/10.1016/j.agrformet.2011.09.010

Seneviratne, S. I., Corti, T., Davin, E. L., Hirschi, M., Jaeger, E. B., Lehner, I., et al. (2010). Investigating soil moisture-climate interactions in a changing climate: A review. *Earth-Science Reviews*, *99*(3–4), 125–161. https://doi.org/10.1016/j.earscirev.2010.02.004

Sheffield, J., Ferguson, C. R., Troy, T. J., Wood, E. F., & Mccabe, M. F. (2009). Closing the terrestrial water budget from satellite remote sensing. *Geophysical Research Letters*, *36*, L07403. https://doi.org/10.1029/2009GL037338

Shuttleworth, W. J., & Calder, I. R. (1979). Has the Priestley-Taylor equation any relevance to forest evaporation? *Journal of Applied Meteorology*, *18*(5), 639–646. https://doi.org/10.1175/1520-0450(1979)018<0639:HTPTEA>2.0.CO;2

Smith, T. J., & Marshall, L. A. (2008). Bayesian methods in hydrologic modeling: A study of recent advancements in Markov chain Monte Carlo techniques. *Water Resources Research*, *44*, W00B05. https://doi.org/10.1029/2007WR006705

Sobol', I. M. (1990). On sensitivity estimation for nonlinear mathematical models. *Matematicheskoe Modelirovanie*, *2*(1), 112–118.

Sobol', I. M. (2001). Global sensitivity indices for nonlinear mathematical models and their Monte Carlo estimates. *Mathematics and Computers in Simulation*, *55*(1-3), 271–280. https://doi.org/10.1016/S0378-4754(00)00270-6

Storn, R., & Price, K. (1997). Differential evolution-A simple and efficient heuristic for global optimization over continuous spaces. *Journal of Global Optimization*, *11*(4), 341–359. https://doi.org/10.1023/A:1008202821328

Su, Z. (2002). The surface energy balance system (SEBS) for estimation of turbulent heat fluxes. *Hydrology and Earth System Sciences*, *6*(1), 85–100. https://doi.org/10.5194/hess-6-85-2002

Talsma, C. J., Good, S. P., Jimenez, C., Martens, B., Fisher, J. B., Miralles, D. G., et al. (2018). Partitioning of evapotranspiration in remote sensing-based models. *Agricultural and Forest Meteorology*, *260-261*, 131–143. https://doi.org/10.1016/j.agrformet.2018.05.010

Tang, Y., Reed, P., Wagener, T., & van Werkhoven, K. (2007). Comparing sensitivity analysis methods to advance lumped watershed model identification and evaluation. *Hydrology and Earth System Sciences*, *11*(2), 793–817. https://doi.org/10.5194/hess-11-793-2007

Taylor, K. E. (2001). Summarizing multiple aspects of model performance in a single diagram. *Journal of Geophysical Research*, *106*(D7), 7183–7192. https://doi.org/10.1029/2000JD900719

ter Braak, C. J. F. (2006). A Markov chain Monte Carlo version of the genetic algorithm differential evolution: Easy Bayesian computing for real parameter spaces. *Statistics and Computing*, *16*(3), 239–249. https://doi.org/10.1007/s11222-006-8769-1

ter Braak, C. J. F., & Vrugt, J. A. (2008). Differential evolution Markov chain with snooker updater and fewer chains. *Statistics and Computing*, *18*(4), 435–446. https://doi.org/10.1007/s11222-008-9104-9

Trambauer, P., Dutra, E., Maskey, S., Werner, M., Pappenberger, F., Van Beek, L. P. H., & Uhlenbrook, S. (2014). Comparison of different evaporation estimates over the African continent. *Hydrology and Earth System Sciences*, *18*(1), 193–212. https://doi.org/10.5194/hess-18-193-2014

Twine, T. E., Kustas, W. P., Norman, J. M., Cook, D. R., Houser, P. R., Meyers, T. P., et al. (2000). Correcting eddy-covariance flux underestimates over a grassland. *Agricultural and Forest Meteorology*, *103*(3), 279–300. https://doi.org/10.1016/S0168-1923(00)00123-4

van de Griend, A. A., & Owe, M. (1994). Bare soil surface-resistance to evaporation by vapor diffusion under semiarid conditions. *Water Resources Research*, *30*(2), 181–188. https://doi.org/10.1029/93WR02747

van Dijk, A. I. J. M., Gash, J. H., van Gorsel, E., Blanken, P. D., Cescatti, A., Emmel, C., et al. (2015). Rainfall interception and the coupled surface water and energy balance. *Agricultural and Forest Meteorology*, *214-215*, 402–415. https://doi.org/10.1016/j.agrformet.2015.09.006

van Griensven, A., van Meixner, T., Grunwald, S., Bishop, T., Diluzio, M., & Srinivasan, R. (2006). A global sensitivity analysis tool for the parameters of multi-variable catchment models. *Journal of Hydrology*, *324*(1), 10–23. https://doi.org/10.1016/j.jhydrol.2005.09.008

Vanrolleghem, P. A., Mannina, G., Cosenza, A., & Neumann, M. B. (2015). Global sensitivity analysis for urban water quality modelling: Terminology, convergence and comparison of different methods. *Journal of Hydrology*, *522*, 339–352. https://doi.org/10.1016/j.jhydrol.2014.12.056

Velpuri, N. M., Senay, G. B., Singh, R. K., Bohms, S., & Verdin, J. P. (2013). A comprehensive evaluation of two MODIS evapotranspiration products over the conterminous United States: Using point and gridded FLUXNET and water balance ET. *Remote Sensing of Environment*, *139*, 35–49. https://doi.org/10.1016/j.rse.2013.07.013

Vinukollu, R. K., Meynadier, R., Sheffield, J., & Wood, E. F. (2011). Multi-model, multi-sensor estimates of global evapotranspiration: Climatology, uncertainties and trends. *Hydrological Processes*, *25*(26), 3993–4010. https://doi.org/10.1002/hyp.8393

Vinukollu, R. K., Wood, E. F., Ferguson, C. R., & Fisher, J. B. (2011). Global estimates of evapotranspiration for climate studies using multi-sensor remote sensing data: Evaluation of three process-based approaches. *Remote Sensing of Environment*, *115*(3), 801–823. https://doi.org/10.1016/j.rse.2010.11.006

Vrugt, J. A., Ter Braak, C. J. F., Diks, C. G. H., Robinson, B. A., Hyman, J. M., & Higdon, D. (2009). Accelerating Markov chain Monte Carlo simulation by differential evolution with self-adaptive randomized subspace sampling. *International Journal of Nonlinear Sciences and Numerical Simulation*, *10*(3), 273–290. https://doi.org/10.1515/IJNSNS.2009.10.3.273

Wang, K., & Dickinson, R. E. (2012). A review of global terrestrial evapotranspiration: Observation, modeling, climatology, and climatic variability. *Reviews of Geophysics*, *50*, L09607. https://doi.org/10.1029/2011RG000373

Yang, J. (2011). Convergence and uncertainty analyses in Monte-Carlo based sensitivity analysis. *Environmental Modelling & Software*, *26*(4), 444–457. https://doi.org/10.1016/j.envsoft.2010.10.007

Yang, Y., Guan, H., Shang, S., Long, D., & Simmons, C. T. (2014). Toward the use of the MODIS ET product to estimate terrestrial GPP for nonforest ecosystems. *IEEE Geoscience and Remote Sensing Letters*, *11*(9), 1624–1628. https://doi.org/10.1109/LGRS.2014.2302796

Yang, Y., Long, D., Guan, H., Liang, W., Simmons, C., & Batelaan, O. (2015). Comparison of three dual-source remote sensing evapotranspiration models during the MUSOEXE-12 campaign: Revisit of model physics: Two-source remote sensing ET model comparision. *Water Resources Research*, *51*, 3145–3165. https://doi.org/10.1002/2014WR015619

Yang, Y., & Shang, S. (2013). A hybrid dual-source scheme and trapezoid framework-based evapotranspiration model (HTEM) using satellite images: Algorithm and model test. *Journal of Geophysical Research: Atmospheres*, *118*, 2284–2300. https://doi.org/10.1002/jgrd.50259

Yang, Y., Shang, S., & Jiang, L. (2012). Remote sensing temporal and spatial patterns of evapotranspiration and the responses to water management in a large irrigation district of North China. *Agricultural and Forest Meteorology*, *164*, 112–122. https://doi.org/10.1016/j.agrformet.2012.05.011

Yao, Y., Liang, S., Li, X., Hong, Y., Fisher, J. B., Zhang, N., et al. (2014). Bayesian multimodel estimation of global terrestrial latent heat flux from eddy covariance, meteorological, and satellite observations. *Journal of Geophysical Research: Atmospheres*, *119*, 4521–4545. https://doi.org/10.1002/2013JD020864

Zhang, C., Chu, J., & Fu, G. (2013). Sobol's sensitivity analysis for a distributed hydrological model of Yichun River Basin, China. *Journal of Hydrology*, *480*, 58–68. https://doi.org/10.1016/j.jhydrol.2012.12.005

Zhang, K., Kimball, J. S., Nemani, R. R., & Running, S. W. (2010). A continuous satellite-derived global record of land surface evapotranspiration from 1983 to 2006. *Water Resources Research*, *46*, D03109. https://doi.org/10.1029/2009WR008800

Zhang, K., Kimball, J. S., Nemani, R. R., Running, S. W., Hong, Y., Gourley, J. J., & Yu, Z. (2015). Vegetation greening and climate change promote multidecadal rises of global land evapotranspiration. *Scientific Reports*, *5*(2), 75–77. https://doi.org/10.1038/srep15956

Zhang, K., Kimball, J. S., & Running, S. W. (2016). A review of remote sensing based actual evapotranspiration estimation. *Wiley Interdisciplinary Reviews: Water*, *3*(6), 834–853. https://doi.org/10.1002/wat2.1168

Zhang, K., Ma, J., Zhu, G., Ma, T., Han, T., & Feng, L. L. (2017). Parameter sensitivity analysis and optimization for a satellite-based evapotranspiration model across multiple sites using Moderate Resolution Imaging Spectroradiometer and flux data. *Journal of Geophysical Research: Atmospheres*, *122*, 230–245. https://doi.org/10.1002/2016JD025768

Zhang, Y. Q., Chiew, F. H. S., Zhang, L., Leuning, R., & Cleugh, H. A. (2008). Estimating catchment evaporation and runoff using MODIS leaf area index and the Penman-Monteith equation. *Water Resources Research*, *44*, L09607. https://doi.org/10.1029/2007WR006563

Zhang, Y. Q., Leuning, R., Hutley, L. B., Beringer, J., McHugh, I., & Walker, J. P. (2010). Using long-term water balances to parameterize surface conductances and calculate evaporation at 0.05° spatial resolution. *Water Resources Research*, *46*, W05512. https://doi.org/10.1029/2009WR008716

Zhao, M., Heinsch, F. A., Nemani, R. R., & Running, S. W. (2005). Improvements of the MODIS terrestrial gross and net primary production global data set. *Remote Sensing of Environment*, *95*(2), 164–176. https://doi.org/10.1016/j.rse.2004.12.011

Zhu, G. F., Li, X., Su, Y. H., Zhang, K., Bai, Y., Ma, J. Z., et al. (2014). Simultaneously assimilating multivariate data sets into the two-source evapotranspiration model by Bayesian approach: Application to spring maize in an arid region of northwestern China. *Geoscientific Model Development*, *7*(4), 1467–1482. https://doi.org/10.5194/gmd-7-1467-2014

Zhu, G. F., Zhang, K., Li, X., Liu, S. M., Ding, Z. Y., Ma, J. Z., et al. (2016). Evaluating the complementary relationship for estimating evapotranspiration using the multi-site data across north China. *Agricultural and Forest Meteorology*, *230–231*, 33–44. https://doi.org/10.1016/j.agrformet.2016.06.006